POI: The Panoramic Optical Imager

UH IfA Small-Telescopes Working Group
Institute for Astronomy, U. Hawaii

Abstract

We discuss the costs of wide-field imaging surveys using ground-based telescopes. In particular, we compare the cost-effectiveness of a single large aperture telescope to that of an array of smaller telescopes. Telescope costs favor small apertures, and the array approach offers many other advantages. CCD costs, on the other hand, favor optically fast designs, and CCD resolution requires that very fast designs be quite large ($D \gtrsim 3$m). However, CCD and electronics costs have fallen to the point that smaller, slower designs with $D \sim 1$m now offer a more cost effective solution, and small telescopes will become still more attractive in the future. We outline a design for a small array of 4 telescopes with $D \simeq 1.3$m and with 7deg^2 field of view costing $\sim \$2M$ per unit. While the collecting area is small, the FOV is huge, making each of these roughly as powerful as SUBARU/SUPRIME, SDSS or CFHT/MEGACAM for wide field surveys. This 'panoramic optical imager' (POI) will be able to fulfill most of the science goals envisaged in the Decadal Review LSST proposal, and will serve as a test bed for future larger arrays.

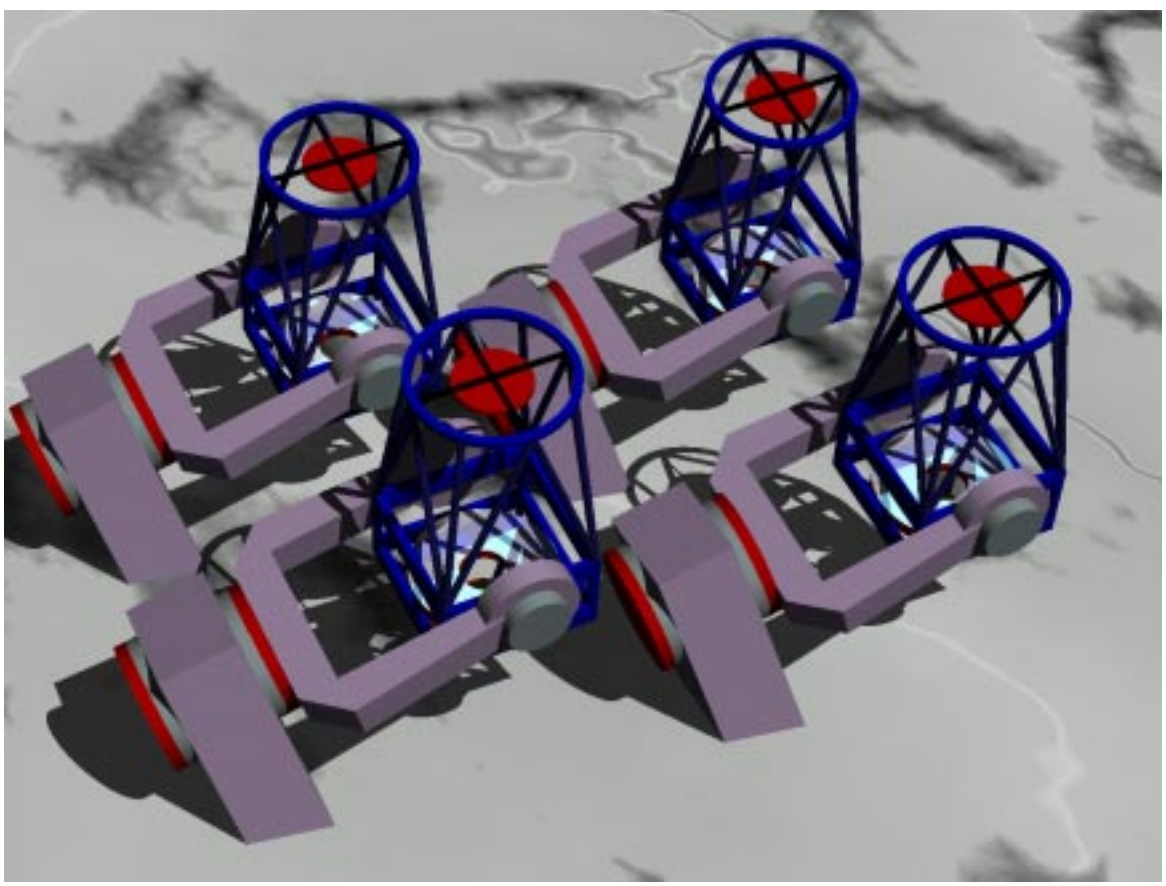

POI: The Panoramic Optical Imager

UH IfA Small-Telescopes Working Group

Nick Kaiser
Hans Boesgaard
Jim Heasley
Klaus Hodapp
Dave Jewitt
Rolf-Peter Kudritzki
Jeff Kuhn
Gerard Luppino
Eugene Magnier
Peter Onaka
Andrew Pickles
Ted Simon
Istvan Szapudi
Dave Tholen
John Tonry

Institute for Astronomy, U. Hawaii

`http://www.ifa.hawaii.edu/~kaiser/poi`

Contents

1 Introduction **6**
1.1 The Digital Revolution in Wide-Field Imaging . . . 6
1.2 Outline . . . 6

2 The LSST **7**
2.1 The Science Case for the LSST . . . 7
2.2 The Dark Matter Telescope . . . 8
2.3 WFHRI . . . 8
2.4 Figure of Merit and Cost Effectiveness . . . 8

3 Telescope Costs **9**

4 Detector Costs **11**
4.1 CCD Costs . . . 12
4.2 Electronics Costs . . . 13

5 Other Advantages of Small Telescopes **13**

6 A Pilot-Project Proposal: The POI **15**
6.1 Optical Designs . . . 15
6.2 Physical Design and Site . . . 16
6.3 Survey Strategy and Scientific Capability . . . 17
6.3.1 NEO Search . . . 18
6.3.2 Cumulative Integrations . . . 19
6.4 Data Processing and Data Management . . . 19
6.4.1 Reduction Pipeline Hardware Requirements . . . 20
6.4.2 Basic Data Products Storage Requirements . . . 22
6.4.3 Software and Data Management Costs . . . 22
6.5 Operation and Maintenance Costs . . . 24
6.6 CCD and Camera Development . . . 24

A Economics of Telescope Costs **26**

B Detector Issues **29**
B.1 Charge-Diffusion . . . 29
B.2 CCD Costs . . . 30
B.2.1 MIT/Lincoln Labs Devices . . . 30
B.2.2 Depleted DDCs . . . 30
B.2.3 IR Detectors . . . 32
B.3 Dewar, Cooler and Shutter . . . 32
B.4 Read-Out Electronics Costs . . . 32

C Sensitivity and Dynamic Range **34**
C.1 Exposure Time Calculations . . . 34
C.2 Trailing Losses . . . 35
C.3 Read-Noise . . . 36
C.4 Dynamic Range . . . 36
C.5 Cosmic Ray Rejection . . . 36
C.6 Drift-Scan Operation? . . . 36

D Finite Aperture Effects **37**
D.1 Diffraction Limit . . . 37
D.2 Fast Guiding . . . 37
D.3 Higher Order Correction . . . 38

E Temporal Sampling **40**

F Image Accumulation **41**
F.1 Introduction . . . 41
F.2 Statistics of the Optimal Summed Image . . . 42
F.3 Flat Spectrum Representation . . . 43
F.4 Image Reconstruction . . . 43
F.5 Point Source Likelihood . . . 45
F.6 Cosmic Ray Rejection . . . 46
F.7 PSF Modeling . . . 46
F.8 Anisotropy Nulling . . . 46
F.9 Choice of Dithering . . . 46
F.10 Pipeline Simulation . . . 46
F.11 Summary . . . 47

G Replicated or Floppy Mirrors? **50**

H Optical Designs **51**
H.1 Modified Bowen-Vaughan Design . . . 51
H.2 Other Designs . . . 52

I Comparison with SNAP-SAT **53**
I.1 Detector Requirements . . . 53
I.2 Performance Comparison . . . 53

J Weak Lensing Efficiency **56**
J.1 Simulations . . . 56
J.2 Shear Analysis . . . 56

K Terrestrial Satellites and Space-Junk **59**
K.1 Bright Satellites . . . 59
K.2 Faint Satellites . . . 59
K.3 Depth of Field . . . 61
K.4 Orbit Determination . . . 62

K.5 Angular Resolution . . . 62
K.6 Dedicated Searches . . . 62
K.7 Curvature of Trails . . . 62
K.8 Conclusions . . . 63

List of Figures

1 Table of Telescope Costs . . . 10
2 POI Common Equatorial Mount Concept . . . 16
3 UH88" Coude Room Installation . . . 17
4 Parallelization of Pipe-Line . . . 21
5 CCD Camera Design . . . 25
6 Charge Diffusion . . . 31
7 Trailing Losses . . . 35
8 FWHM vs Aperture . . . 37
9 PSF Profile vs Aperture . . . 38
10 Fast Guiding Efficiency . . . 39
11 Aliasing in Good Seeing . . . 44
12 Image Accumulation Pipeline . . . 48
13 Matched Image Subtraction . . . 49
14 Physical Layout . . . 51
15 Spot Diagrams . . . 52
16 SNAP Efficiency . . . 54
17 HDF WL Simulations . . . 58
18 Satellite Detection Limits . . . 61

1 Introduction

1.1 The Digital Revolution in Wide-Field Imaging

Electronic detectors (CCDs) developed in the '70s and 80's completely revolutionized many areas of astronomy. The early detectors, however, were too small for wide-field imaging, and this field fell into decline.

Recently the situation has changed as the cost of CCDs has fallen dramatically. Cameras with up to 100M pixels have been deployed on a number of large telescopes, and are generating images of huge coverage and depth. A closely related development is a move towards dedicated survey instruments such as 2MASS and SDSS.

In this 'white-paper' we argue that the low current cost of CCDs and associated electronics — and the still lower expected costs in the near future — make arrays of small telescopes the preferred solution for wide-field imaging.

In outline, the argument rests on the following considerations: First, as is well known, the cost of telescopes rises faster than the collecting area. Thus, for imaging surveys which accept the natural seeing, telescope costs favor 'distributed apertures'. Second, while multiple telescope designs may appear to be inefficient in that they require multiple cameras, these cameras can in fact be made smaller than has been common in the past, so the inefficiency is less than one might imagine. Clearly, for a given total light-collecting area, the total area of detectors is just proportional to the square of the focal ratio F, so if one were simply to scale down a large telescope design then the total area of detectors would be fixed. The limiting factor here is the physical resolution of the detectors — which must not degrade the seeing — but we find that there is still considerable scope for miniaturization. Finally, the cost of read-out electronics scales linearly with the number of telescopes and inversely with integration time. This is a disadvantage for arrays of telescopes if used for applications such as NEO searches which require fairly short integration times. However, this is not a crippling problem since the cost of electronics is a small fraction of the total cost.

We would argue that the size of the individual apertures is a parameter to be varied just like any other in order to optimize the design. In this optimization one must consider not only financial considerations noted above, but also consider construction time, environmental impact etc. These again favor distributed apertures. This paper consists mostly of a preliminary attempt to determine this optimal solution. There are considerable uncertainties in many of the the needed inputs, but it appears that currently small telescopes with $D \simeq 1$ m are close to optimal.

1.2 Outline

This document is divided into two parts; the main text which elaborates on the points mentioned above (and others), and a series of appendices containing more details and calculations to back up the numbers used in the argument. In the main text, we first review the science case for the 'Large-Synoptic Survey Telescope' (LSST) and mention some proposed designs. We then discuss in turn telescope and detector costs, and list various other considerations.

We then present an outline proposal for a small array of 4 telescopes with $D \simeq 1.3$m and with 7deg^2 field of view (which we estimate would cost $\sim \$2M$ per unit). While the collecting area is small, the FOV is huge, making each of these roughly as powerful as SUBARU/SUPRIME,

SDSS or CFHT/MEGACAM for wide field surveys. This 'panoramic optical imager' (POI) will be able to fulfill most of the science goals envisaged in the Decadal Review LSST proposal, and will serve as a test bed for future larger arrays.

2 The LSST

2.1 The Science Case for the LSST

The NRC AASC Decadal Review for Astronomy has endorsed a dedicated large imaging survey as a prioritized major initiative for the coming decade. To quote from their report "Astronomy and Astrophysics in the New Millennium"

> The committee recommends the Large-aperture Synoptic Survey Telescope (LSST), a 6.5m class very-wide-field ($\sim$ 3deg) telescope that will produce a deep ($\sim$ 24th magnitude in a single optical band) digital map of the visible sky every week. Not only will LSST carry out an optical survey of the sky far deeper than any previous survey, but it will also add the new dimension of time and thereby open up a new realm for discovery.

The reviewers estimated a cost for this project of $170M, and the scientific output from a survey of this scale would include:

- Asteroids/Near-Earth Objects
  - Complete catalogs: 90% of 250-meter size 'killer asteroids' to be detected within the first decade at a rate of $\gtrsim 100$ per day.
  - Origin and fate of small bodies in the Solar System.
  - Relation to Kuiper Belt and Trans-Neptunian Objects.
  - Solar-system dynamic structure.
- Planet Search
  - 100,000,000 stars to be monitored.
  - Planet detection from occultation and micro-lensing.
- Galactic Halo and Disk Components
  - Search for low-luminosity White Dwarfs of ~ 0.5 solar masses.
  - Discovery of $\sim 100,000$ Brown Dwarfs.
- Supernovas
  - Discover $\sim 100,000$ per year.
  - Heavy element abundance question.
- Galaxy Clustering
  - Two-dimensional maps of slices of the universe to redshift $z \sim 1$.

  - Feeder for next generation 3-dimensional spectroscopic redshift surveys.

- Weak-Lensing Studies
  - Distribution of dark matter on scales from $\sim$ 10kpc to $\sim$ 100Mpc.
  - Direct measurement of power-spectrum of mass fluctuations.
  - Independent constraints on cosmological theory.

- Transients
  - Gamma-ray bursts.
  - Lensed quasars.
  - Vast new discovery space for currently unknown optical transients.

- Space-Junk
  - Detection and monitoring of satellites and space debris.

2.2 The Dark Matter Telescope

One proposal for a dedicated large-scale survey instrument is the "Dark-Matter Telescope" (DMT) (Dark Matter Telescope Web Site 1999, Tyson & Angel 2000, Angel et al. 2000). It features a modified 'Paul-Baker' or 'Mersenne-Schmidt' optical design like that proposed by Willstrop (1984). It has three mirrors, a curved focal plane and two refractive elements. The primary mirror diameter is 8.4m, considerably larger than the 6.5m suggested by the decadal review, but the effective collecting diameter is 6.9m, and it provides a 3-degree diameter FOV. The DMT web-page gives an estimated cost $C \simeq$ \$120M (though the Decadal Review assigned a figure of \$170M including operating costs for their smaller LSST concept). It is proposed to operate in the optical and near-IR, though the IR detector technology remains quite uncertain. The DMT would be able to detect a point source with V-band magnitude of $V = 24$ at the 5-sigma level in about 20 seconds.

2.3 WFHRI

An alternative proposal is the WFHRI; an array of small telescopes with low order adaptive optics image correction to provide very high resolution images (Kaiser, Tonry, & Luppino 2000, WFHRI Web Site 1999). The design requires orthogonal transfer CCDs (Tonry, Burke, & Schechter 1997), with rather small pixels, and has a rather sophisticated algorithm to deal with the atmosphere.

2.4 Figure of Merit and Cost Effectiveness

For survey instruments which accept the natural seeing, the key figure of merit is simply the *etendue*; the product of the collecting area A and the solid angle of the field of view Ω (though for some applications such as transient object searches and rapidly moving objects there are other considerations — we discuss these in appendix E). With linear detectors like CCDs, and

assuming sky noise dominates, the amount of science generated in time t is just proportional to $A\Omega t$. One night on a $A = 100\mathrm{m}^2$ telescope with a $1\mathrm{deg}^2$ FOV generates exactly as much science as one night on a $A = 1\mathrm{m}^2$ telescope with FOV $\Omega = 100\mathrm{deg}^2$. Many nights per year on a small telescope is exactly equivalent to one on a large telescope etc. It is all very boring and unromantic, but the *etendue* at least allows one to quantify unambiguously the relative cost effectiveness of different instruments.

The (inverse of the) cost-effectiveness of a survey instrument is the *specific cost* χ, which we will define as the capital cost of the instrument divided by the rate at which science is generated

$$\chi = \frac{\mathrm{cost}}{A\Omega}. \tag{1}$$

One might argue that the numerator should in fact be the interest on the capital cost plus operating costs, but these both tend to scale as a multiple of the capital cost, so (1) is adequate for comparing different designs.

The estimated specific cost for the 6.5m LSST concept (including operating cost) is $\chi_{\mathrm{LSST}} = 1.1\$\mathrm{M/m}^2/\mathrm{deg}^2$ (see table 1). Angel and Tyson estimate a lower specific cost for the 8.4m DMT of $\chi_{\mathrm{DMT}} = 0.46\$\mathrm{M/m}^2/\mathrm{deg}^2$. If achieved, this would be much less than for SUBARU/SUPRIME ($\chi \simeq 27$) (Subaru Suprime-Cam Web Site 1999) or CFH12K[1] ($\chi \simeq 13$) or CFHT with MEGA-CAM[2] ($\chi \simeq 5$), and compares favorably with the UK VISTA proposal (estimated $\chi \simeq 1.4$) (Vista Web Site 1999). The WFHRI would be somewhat more costly per unit *etendue*, but for some applications (weak lensing, accurate object positions) the sharper images convey a large advantage in efficiency. For such goals the only competitive alternative is a space mission like SNAP-SAT[3].

3 Telescope Costs

In the WFHRI proposal, the size of the telescopes ($D \simeq 1.5$m) is dictated by matching the adaptive optics system to the atmospheric seeing. Here we ask: What is the optimal telescope size for ground based large-scale surveys which accept the natural seeing? The answer to this question involves a play-off between telescope costs and detector costs. A more detailed discussion of the relevant factors is given in appendix A. Here we simply observe that the US Naval Observatory recently purchased a $f/4$ 1.3m telescope, with $1^\circ.7$ diameter FOV from DFM Engineering[4]. The design (Melsheimer & MacFarlane 2000) is a Ritchey-Chretien with corrector plate similar to, but somewhat faster than, the Bowen-Vaughan Las Campanas 40" design. Such a telescope can be purchased for around \$900K, and the cost per unit collecting area is about $\$0.53\mathrm{M/m}^2$, about a factor 10 less than the LSST and a factor 5 less than the DMT estimate. The FOV here is smaller, so the specific telescope cost is $\chi_{\mathrm{tel}} \simeq 0.29\$\mathrm{M/m}^2/\mathrm{deg}^2$, but this is still considerably better than the DMT, and unit costs for multiple orders would be smaller still. (We will consider detector costs presently).

It is possible to extend the field of view by making the design slower, as in the Las Campanas 40", or adding a second refractive correcting element, as in the SDSS telescope, with little

[1] `http://www.cfht.hawaii.edu/Instruments/Imaging/CFH12K`
[2] `http://www.cfht.hawaii.edu/Instruments/Imaging/Megacam`
[3] `http://snap.lbl.gov`
[4] `http://www.dfmengineering.com`

name	D	A/m^2	Ω/deg^2	$A\Omega$	C	$\chi = C/A\Omega$
LSST	6.5m	26.54	7.1	188	\$170M	1.1
DMT	8.4m	37.4	7.1	260	\$120M	0.46
SDSS	2.5m	3.9	1.55	6.0	\$120M	20.0
VISTA	4.0m	10.0	2.3	23	\$40M	1.7
SUBARU	8.2m	44.3	0.2	8.8	\$350M	39
CFH12K	3.6m	8.1	0.375	3.0	\$50M	16
MEGACAM	3.6m	8.1	1.0	8.1	\$50M	6.1
USNO	1.3m	1.1	2.2	2.3	\$1.4M	0.60
Meade 16"	0.4m	0.125	0.25	0.031	\$45K	1.42

Figure 1: Comparison of performance and cost of some existing and proposed photometric survey instruments. The LSST cost includes operating costs. The USNO cost assumes \$500K for detector. The Meade 16″ includes \$30K for a 4K × 4K camera from Apogee. Note that for a multi-purpose system like SUBARU, the specific cost for *imaging* is the total system cost including *all* instruments, divided by the science output per unit time while used for imaging. To see that this is rational, one could say that a \$300M dollar system used equally for three different projects is like three \$100M dollar single purpose instruments, so the cost per project is three times less, but the rate of science output for each project is also correspondingly three times lower. In general, the total system specific cost is the inverse of the average inverse specific cost for each project, weighted by the fraction of time that the project is active. Vignetting/obscuration losses of 20% have been assumed for most of these designs.

increase in construction cost. Both designs deliver a 3-degree diameter field of view. We have modified the Bowen-Vaughan design to $f/5.4$ and still obtain very good image quality over the full 3° field ($\Omega \simeq 7\mathrm{deg}^2$). One such telescope with $D = 1.3$m would have $A\Omega \simeq 7.5$, about as powerful as SUBARU/SUPRIME (8.8) or CFHT/MEGACAM (8.1) and one third as powerful as VISTA. With a 3 degree field of view and $C_{\mathrm{tel}} = \$900\mathrm{K}$ the specific telescope cost is $\chi_{\mathrm{tel}} \simeq 0.1\$\mathrm{M}/\mathrm{m}^2/\mathrm{deg}^2$, about a factor 5 better than the DMT. Vignetting losses of $\sim 25\%$ in the BV design push this up, but discount for multiple orders will offset this.

Further gains in cost effectiveness result if we consider performing a survey with a large *array* of small telescopes. An array of 28 $D = 1.3$m 3deg FOV telescopes would have the same collecting area and *etendue* as the DMT. With this level of mass-production there should be considerable economies of scale in many aspects of the manufacturing process, and it may then be worth considering alternative technologies such as light-weight or replicated mirrors, novel mounts etc.

For very small telescopes the image quality is degraded by diffraction, especially in the red. For apertures of the size considered here, however, the effect is unimportant (see appendix D).

To summarize the arguments presented in appendix A below, optics and materials science considerations generally tend to favor arrays of small telescopes for wide field surveys. Conventional small telescopes as are readily available from commercial vendors outperform large telescope designs, and for a project of the scale envisaged by the decadal review the possibilites for cost savings from new technology are considerable. However, an obvious missing factor in the above analyis is clearly detectors costs, which we now consider in more detail.

4 Detector Costs

Detector costs are a critical factor in the comparison between small and large telescopes. We understand that the USNO budgetted \$1.8M for a detector for their 1.3m, or about twice the cost of the telescope. Worse still, the cost of the CFH12K ($\Omega = 0.375\mathrm{deg}^2$) was around \$1M, and the cost of the MEGACAM/MEGAPRIME project is around \$14M for a $\Omega \simeq 1\mathrm{deg}^2$ FOV (though this includes a substantial component for the correcting optics). These are sobering numbers indeed, and would seem at face value to severely undermine the cost-effectiveness of small telescopes. However this is quite misleading for number of reasons.

- Plate scales (microns per arcsec on the focal plane) have been determined not so much by the physics of the detectors as by the need to match large-telescope designs. For small telescopes the plate scale can be smaller and the CCD costs correspondingly lower.

- The costs of most existing wide-field detectors has been inflated by the drive to large rectangular detectors which poorly fill circular wafers and, for thinned deviced particularly, suffer rather poor yields. Yield can be increased by using wafer-scale arrays of smaller detectors, where one accepts a small fraction of non-functioning detector cells.

- A significant reduction in CCD cost is promised by non-thinned depleted devices as being developed by the LBL group. A factor $\gtrsim 2$ reduction in cost should be realised with the development of devices for the 'One Degree Imager' for the WIYN telescope.

- All cameras to date have been one-off designs with a large R+D cost component. The technology is now fairly mature, and, with an array of telescopes, design and software development costs etc are distributed over multiple units.

- Most detectors have been designed to operate over a wide range of wavelengths in order to fulfill many science objectives. With a large array of telescopes, detectors can be optimised for a single passband.

- An analog of 'Moore's law' has resulted in huge decreases in cost of detectors with time. For example, the 4K $\times$ 4K MOCAM detector was a huge effort consuming many man-years of effort, yet was rendered obsolete almost immediately after commissioning by the UH8K. A complete 4K $\times$ 4K camera with performance similar to that of MOCAM can now be purchased from Apogee for $\sim$ \$30K. Telescopes have relatively stable costs and are an investment that will yield returns over many years, if not decades. It makes no sense to design wide-field imaging systems for current detectors, much less last year's. Rather than making a system that can cover all pass-bands it is better to get started with whatever is most economical today — i.e. broad-band optical imaging. One can then anticipate future upgrades to say IR detectors, OTCCDs for WFHRI imaging, detectors with temporal/energy resolution etc as these come along. These developments will likely occur on a time-scale shorter than the planning/construction time for a large telescope.

- Imaging detector costs are still a small fraction of the total system costs for most large telescopes, so quite understandably more thought and effort has gone into beating down the cost of the major components — the telescope and enclosure. For wide-field imaging the situation is very different, and we now look more carefully at the likely costs for optimized current and future detectors. More details can be found in appendix B.

4.1 CCD Costs

Detector costs have two major components: the CCDs and the read-out electronics. Both of these scale linearly with the solid angle of the FOV Ω (so the specific detector cost is essentially independent of Ω) but it is useful to separate them since the former depends also on the plate scale, and thereby on the f-ratio of the telescope (which we shall denote by F). The cost of read-out electronics is independent of F, but depends critically on the integration times dictated by the scientific objectives.e

To a first approximation, the cost of CCDs is proportional to the *area* of silicon (rather than the number of pixels). This means that for a given telescope design, with a certain f-ratio, the CCD cost per unit collecting area is independent of the telescope aperture, since smaller telescopes have proportionately smaller detectors. However, if we make the telescope too small, then we will eventually run into one of two limits: either the telescope will become diffraction limited, or the plate scale will become so small that the detector cannot resolve the PSF.

In designing a camera which is optimal for small telescopes, a fundamental limitation is therefore the physical resolution of the detector. This must not compromise the angular resolution provided by the atmosphere. The resolution limit arises from charge diffusion. We review this in more detail in appendix B, where we show that the predicted Gaussian charge probability distribution scale length for 150μm thick LBL style fully depleted device is $\sigma_{\rm diff} \simeq 3\mu$m (see §B.1), and if we require that this not degrade the seeing width by more than 10% gives the constraint on the plate-scale

$$s \geq 5 \left(\frac{\sigma_{\rm diff}}{3.0\mu{\rm m}}\right) {\rm m} = 24 \left(\frac{\sigma_{\rm diff}}{3.0\mu{\rm m}}\right) \left(\frac{\mu{\rm m}}{\rm arcsec}\right). \tag{2}$$

We have assumed here good seeing with FWHM $= 0''.6$. Note that this is smaller by about a factor 3 than the plate-scale used in SUPRIME and the CFH12K, and about a 2 smaller than assumed for the DMT. This converts to very large savings (by a factor $\sim 4-10$) in the cost of CCDs since a much greater solid angle can be imaged onto a given physical area.

The plate-scale d, aperture D and f-ratio are related by $s = DF$, so we have the corresponding constraint on the f-ratio

$$F = s/D \geq \left(\frac{D}{5{\rm m}}\right)^{-1} \left(\frac{\sigma_{\rm diff}}{3\mu{\rm m}}\right). \tag{3}$$

To properly sample $0''.6$ seeing with $\sigma_{\rm diff} = 3\mu$m therefore requires a focal length $f \gtrsim 5$m.

The specific CCD cost is

$$\chi_{\rm CCD} \equiv \frac{C_{\rm CCD}}{A\Omega} = \frac{c_{\rm CCD} s^2 \Omega}{\pi (D/2)^2 \eta \Omega} = \frac{4}{\pi} \eta^{-1} c_{\rm CCD} F^2, \tag{4}$$

where $1-\eta$ is the fraction of light lost to vignetting, and $c_{\rm CCD}$ is the cost per unit area of CCDs. Thus detector cost considerations favor *faster* designs. Since the limit on the f-ratio (3) from the CCD detector resolution depends inversely on the aperture, these considerations also indirectly favor large apertures. For example, applied to Willstrop's 3-mirror $f/1.6$ Mersenne-Schmidt design this gives a limit on the aperture $D_{\rm min} = 3$m. However, using a larger aperture than this confers no benefit in terms of CCD costs, and imposes a severe penalty in increased telescope cost.

We review CCD costs in §B.2. Thinned CCDs from MIT/Lincoln Lab as used in many recent large instruments (and as supplied to the DEIMOS project specifically) had a cost per unit area of $c_{\rm CCD} \simeq 13\$\mathrm{M/m^2}$ with corresponding specific cost $\chi_{\rm CCD} \simeq 0.08\eta^{-1}(F/4)^2\$\mathrm{M/m^2/deg^2}$ comparable to the specific telescope cost above. Yield can be increased by using mosaics of smaller units. Increases in yield may also come from improved manufacturing and thinning techniques. In what follows we will adopt a cost per unit area for CCDs of

$$c_{\rm CCD} \equiv \frac{C_{\rm CCD}}{A_{\rm CCD}} \simeq \$6\mathrm{M/m^2} \tag{5}$$

i.e. about a factor two less than the DEIMOS chips cost. We feel this is a fairly reasonable extrapolation of the recent history of MIT device costs, and we note that the depleted CCDs as pioneered by the LBL group could reduce costs still further. This says that detectors are cheap, and heavily swings the balance in favor of small telescopes. The specific CCD cost is then

$$\chi_{\rm CCD} \simeq 0.037\eta^{-1}(F/4)^2\$\mathrm{M/m^2/deg^2}. \tag{6}$$

Note that (6) only applies to *optical* detectors, and *infra-red* detectors are much more expensive. It is worth keeping in mind however that costs of all detectors will only decrease in the future.

4.2 Electronics Costs

Read-out electronics are another major cost factor, particularly for applications like near-earth object searches where short integration times are desirable. In §B.4 we show that to achieve 30-second read-out times (as desirable for 1-minute integrations say) using conventional Leach controllers gives a specific cost for the read-out electronics of

$$\chi_{\rm elec} \simeq 0.036\eta^{-1}(D/1.3\mathrm{m})^{-2}\$\mathrm{M/m^2/deg^2}. \tag{7}$$

The UH IR camera controllers could also be used and would have very similar costs. This figure is about a factor three less than the specific telescope cost for our canonical design. However, this is another area where there could be large cost savings. The IfA has considerable expertise in this area, and even for the pilot project, the scale of mass production is such that application specific integrated circuits (ASICs) are economically viable. Note that development of these electronics are also being driven by numerous other projects such as the imager for the WIYN telescope and projects such as SNAP-SAT.

5 Other Advantages of Small Telescopes

There are a number of other factors which generally favor arrays of small telescopes rather than single telescope designs.

- Construction time-scale — the project outlined below could start operation in a couple of years and would already present a huge increase in power as compared to all other facilities. Large telescope projects typically take on the order of a decade from planning to operation.

- Low risk. The pilot project costs below are based on proven technology.
- Diversity of operation modes — a large array of telescopes can always be operated much as a single large telescope of the same *etendue* by pointing all the telescopes at the same point in the sky. However, one also has the alternative of observing in a shallower but wider field mode, which is better for searching for transient objects (see §E) and for monitoring time varying sources. An array also allows the option of simultaneous multi-color observations
- Small telescopes have better *dynamic range*, in the sense that the saturation limit for bright objects is higher.
- Groups of small telescopes can simultaneously image the same patch of sky. This results in vastly superior cosmic-ray rejection; a critical factor for NEO searches.
- Future development and upgrade path:
  - Arrays of telescopes are readily expandable, and cost scales at most with number of telescopes.
  - WFHRI imaging when OTCCDs become available.
  - Upgrade to infra-red or detectors with good time and/or energy resolution.
  - Interferometry.
- Guiding can be used effectively to correct for low-altitude turbulence (this is not possible for large telescopes) and also 'wind-shake'. This *may* be possible for large telescopes, but it by no means guaranteed since it requires that the wind driven oscillations only cause tilt of the mirror surface and that all higher oscillation modes not be excited. This is discussed further in §D.
- Simple designs offer better image quality in terms of the *isotropy* of the PSF, which is important for e.g. weak lensing applications. This is especially true of the Couder telescope (Willstrop 1983), which is worthy of more careful study.
- Interference filters perform better with slow designs.
- Small telescopes can be housed in low-profile enclosures. These have significantly lower environmental impact. However, an open question here is whether this will degrade the seeing. Some site testing is needed to firmly resolve this.

The main factor, however, is that the lower specific cost means one can potentially do a lot more science for the same amount of money, or, less attractively, the same science for less money.

6 A Pilot-Project Proposal: The POI

Large arrays of small telescopes offer potentially huge gains in cost-effectiveness and many other advantages. Here we propose as a pilot project a 'Panoramic Optical Imager' (POI) consisting of 4 telescopes. The motivations for this choice (rather than 1 or 100 for example) are the following

- This number of telescopes allows the R+D costs (primarily in the detector area, but also in telescope and software design) to be spread over a reasonable number of units.
- It will allow a rigorous proof of concept and provide a test-bed for a future, more extensive arrays. It will provide the detailed characterisation of the atmosphere required for e.g. efficient implementation of WFHRI imaging or higher order correction for low-level turbulence.
- At the same time it will provide a dedicated facility of unparalled power for performing wide-field imaging and, as we shall see, will make possible most of the science goals envisaged by the decadal review.

We shall not assume any major gains from new technology and will base the cost estimates firmly on readily available equipment.

6.1 Optical Designs

As discussed, there are many options for small, wide-field telescopes. These include the Willstrop 3-mirror designs, and also simple designs such as Couder, Schmidt and even fully refractive designs. Another option is to use off-axis designs. With seed funding, all of these will be explored in detail. To focus the discussion we consider here RC + Gascoigne corrector designs as these offer an 'existence proof' of what can be done and have well defined and demonstrated costs.

One design we have explored is a modification of the Bowen & Vaughan (1973) design for the $40''$ at Las Campanas, with $f/5.4$ rather than $f/7$. It has two aspheric mirrors and a Gascoigne corrector plate mounted in front of the detector (which is flat). It is also very similar to the DFM design for the USNO 1.3m. More details are given in appendix H. The design has a compact profile.

We have also explored a 'Sloan-clone' which is similar but has a second refractive corrector mounted directly in front of the focal plane (the CCDs could be glued to the flat rear surface). The image quality for this design was not quite as good.

These designs are preliminary — we need to incorporate baffling and also properly include the effect of the dewar window.

The plate scale for the BV design is 34μm/arcsec, and is somewhat larger than what we have estimated to be the minimum consistent with depleted CCD resolution. It is compatible with the lower resolution found for MIT chips. This pushes up the specific CCD costs to around $\chi_{\rm CCD} \simeq 0.06\$\mathrm{Mm}^{-2}\mathrm{deg}^{-2}$, but as there is still some uncertainty in the actual resolution for MIT chips, this probably safe for the present. With the above figures, the main components of the system cost are telescope, CCDs and electronics, and give a total specific system cost

$$\chi_{\rm total} = \chi_{\rm tel} + \chi_{\rm CCD} + \chi_{\rm elec} \simeq (0.1 + 0.06 + 0.03)\$\mathrm{Mm}^{-2}\mathrm{deg}^{-2} \simeq 0.19\$\mathrm{Mm}^{-2}\mathrm{deg}^{-2} \qquad (8)$$

which is a factor $\simeq 2.5$ better than the *estimated* cost effectiveness for the DMT (and possibly much better than the *actual* cost effectiveness for such a system were it to be built). The cost per telescope is around \$1.7M, spread roughly equally between telescope and detector costs. If we were to base the CCD costs on the actual price for the DEIMOS devices this would push the price up to around \$2.5M per telescope.

6.2 Physical Design and Site

The telescope costs quoted above are based on actual costs for the USNO telescope, which has an equatorial mount. There may be some cost savings by going to alt-az mounts with an instrument rotator, or by having the telescopes share a common mount, as illustrated in figure 2. In this type of design each telescope would be guided independently and would also have a small amount of angular control so as to allow either observations of a single 7.1deg^2 patch or four contiguous patches say.

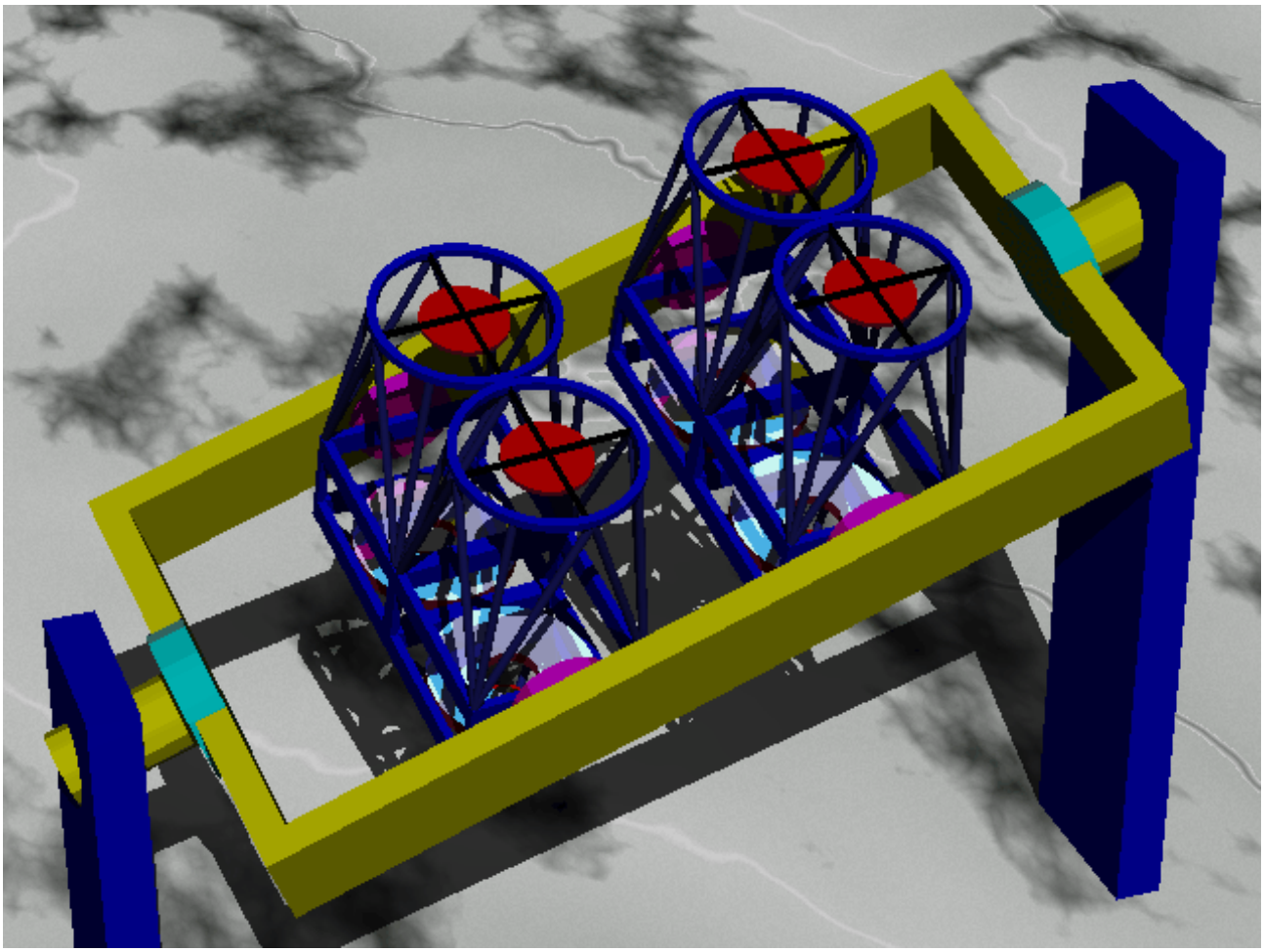

Figure 2: Illustration of several telescopes sharing a common mount.

Two possible sites for such an instrument are a) the site currently occupied by the UH24" and b) the Coude room of the UH88". The former has been designated in the MK Master Plan as a possible site for a $2-3$m class telescope. The latter has the great advantage that the

building is already in place. For the design shown in the figure, the dome starts to obstruct the beam at about 30deg from the North polar axis, resulting in a loss of access to about 7% of the sky. An advantage of this site is that the operator of the UH88" can also monitor the survey telescope.

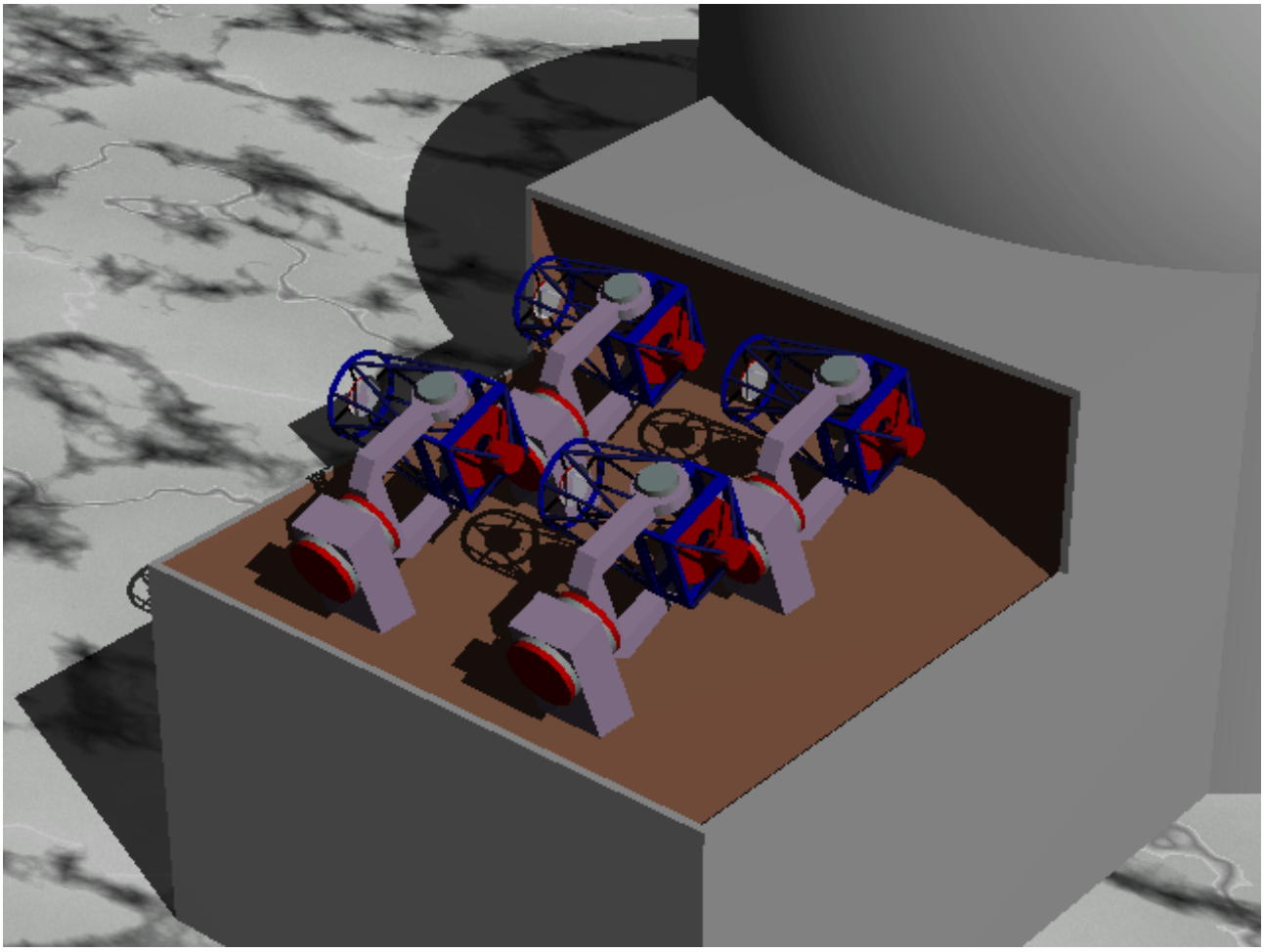

Figure 3: Illustration of how the four POI telescopes could be housed within the Coude room at the UH88" site.

A detailed estimate of the cost for the domes for the Keck outrigger telescopes are on the order of $0.75M per unit. These are not much smaller than would be needed to house the 4 smaller telescopes considered here, indicating a cost on the order of $\sim$ $1M for a new enclosure and less for a refurbished UH88" Coude room.

Note that according to the Master Plan, an array of telescopes used in this manner counts as a single facility.

A high priority is to perform site testing to establish the actual image quality at these sites.

6.3 Survey Strategy and Scientific Capability

6.3.1 NEO Search

The choice of observation strategy for NEO search strategy is driven by two factors: the speed the objects move, and the desire to avoid the 'picket fence problem' (observing field A while the object lies in field B and *vice versa*).

Typical angular velocities for earth crossing asteroid detections are around $\dot{\theta} \simeq 0^\circ.3$ per day (Bowell and Muinonen, in Gehrels, Matthews, & Schumann (1994)). Equivalently they move about $0''.012$ per second, so they move the size of the seeing disk ($0''.6$) in about one minute. Longer integrations than this are relatively inefficient, as the detectable object flux increases as the square root of integration time.

The Decadal Review specification for the LSST is that it should be able to survey the whole visible sky to $R = 24$ in a week. Integration times for the 4-shooter to reach this flux are given in §C.1. These calculations assume the four telescopes are pointed at the same patch of the sky. With typical color $V - R = 0.4$, it takes us about 120 seconds to detect such an object in either V or R and about 60 seconds for a broader $V + R$ filter. These values assume FWHM $= 0''.6$ seeing. See §C.1 for more discussion. As discussed in §C.5 below, a great advantage of this mode of observation is efficient cosmic-ray rejection.

If the telescopes are housed in the $88''$ Coude room then the Northern declination limit is $+60^\circ$. If we restrict ourselves to zenith distances less than 50° the Southern limit is -30°. This band encompasses 68% of the sky, or around $28,000\mathrm{deg}^2$.

If we assume 60 second integration and 30 second readout time, then we obtain 40 exposures per hour, or about 400 exposures in a 10 hour night. With a 3deg diameter FOV this allows us to cover $2,800$ square degrees of sky per night. In 10 hours, an area of $\sim 11,000\mathrm{deg}^2$ of the $-30 : +60$ declination range will pass overhead, of which we could cover about one quarter on any single night. One possible strategy that suggests itself is to survey 1/4 of the declination range each night and step by say 1/12 of the range each night to give three detections for typical objects separated by 24 hours.

This strategy suffers very little from the picket-fence problem. If we scan from North to South with steps of $\Delta\theta$ from night to night (so we survey a region $3 \times \Delta\theta$ wide each night) then an object would have to move North at a speed of at least $\dot{\theta} = 3\Delta\theta/\mathrm{d}$ in order to escape detection at all. The probability of detection for a faster object is $(\dot{\theta}/(\Delta\theta/\mathrm{day}))$. Thus, an object must be moving fast — and therefore be very close — in order to slip through the net. Such objects will therefore typically be discovered at some later time when they are farther away. Objects with $\dot{\theta}$ in the range $2 - 3\Delta\theta/\mathrm{d}$ will be detected once or twice. These will leave a trail $18 - 36$ arc-seconds long. If they are detected twice the pairs of trails are easily matched up, and an accurate prediction can be made for the future location. More slowly moving objects will be detected three times. While the typical objects will only leave very short trails, the fact that they appear three times (moving on straight lines in 3-D angle-time space) again means that the motions for all objects can be determined.

This assumes that the 4 telescopes are pointed at the same patch of sky. What about the alternative of pointing at 4 contiguous fields and surveying the sky at four times the rate (but to a limiting flux 2 times higher)? As discussed in §E this shallow-but-wide strategy is beneficial for detecting very short transients, but it is disadvantageous for killer asteroid searches since the flux limit is poorer, and there seems to be little advantage in detecting an object 12 times in a dark run rather than 3 times. This argues in favor of simultaneous rather than contiguous field observing mode. Generalizing to an array of many telescopes, we feel that one would want to

take advantage of the superior cosmic-ray rejection offered by simultaneous observing in groups of say 3-4 telescopes, but this leaves open the option of whether to point *all* the telescopes at the same patch. This is probably the preferred choice for asteroid searches since it allows one to detect fainter objects, but for transient searches one would probably want to spread the groups apart.

With the strategy outlined above, we find that in the course of one dark run the whole of the available sky — a patch ~ 100 degrees on a side — would be covered once in this triple-pass fashion.

Since objects move $\sim$ 9deg per month, it is not necessary to perform the NEO search every dark run, since one will largely re-detect known objects. This would yield better orbit parameters, but an alternative would be to follow detected objects with one or more auxiliary telescopes (which would not need a huge camera). This means that the NEO searches can happily co-exist with other survey work.

6.3.2 Cumulative Integrations

We would envisage alternating the broad-filter NEO observations with other wide field observations in other passbands; say in B and in I. An important product of these scans will be full-sky cumulative images. In say 180 clear dark nights the complete $28,000\mathrm{deg}^2$ survey region would be covered about 18 times. This results in a cumulative image with limiting magnitude for static sources of about $V_{\mathrm{lim}} \simeq 25.5$.

This can be compared with the SDSS limiting magnitude goal of about $V \simeq 23.2$ (more precisely $g' = 23.3$ and $r' = 23.1$) over the North galactic cap region ($10,000\mathrm{deg}^2$), though their survey is in 5 passbands.

There are various other options involving smaller patches of the sky. For example, one could observe say 14 patches around the sky to give a total area of $100\mathrm{deg}^2$. In 120 dark nights, each field could be observed for about 85 hours, to reach a limiting magnitude of $V_{\mathrm{lim}} \simeq 28.5$. The limit would be somewhat brighter for a multi-color survey. It would be most efficient to interleave observations of different types.

6.4 Data Processing and Data Management

The process of extracting useful scientific results from a survey of this kind can be broken into two separate parts: First there is the pipeline required to process the raw images and generate the basic data products, in this case the accumulated images and catalogues of transients. Then there is the database interrogation software required to facilitate the extraction of science from the database.

Here we shall focus on the first part of this problem. We first describe the scope of the problem and estimate the computing power and storage requirements etc. We then review the extensive software resources already available to us for this task, and estimate the costs of managing the data processing.

The database engineering aspects of this problem are much less advanced. The costs in this area could potentially be huge. However, the problems here are common to *all* future large survey programs. For this reason, the Decadal Review has recommended that this 'grand computing challenge' be coordinated in a unified way under the auspices of a 'National Virtual Observatory' (NVO). The NVO is the top ranked small project, and carries an estimated price

tag of $\sim$ \$60M. The NVO will be a distributed entity. The POI will be a major node of the NVO, and attention needs to be paid to ensuring that the output of the POI pipeline couple efficiently to the NVO, but we will not need to duplicate the data-mining technology that the NVO will produce.

6.4.1 Reduction Pipeline Hardware Requirements

A 3deg diameter field with $0''.3$ pixel scale contains 1.02×10^9 pixels. The NEO search application requires that we take exposures every 90 seconds. This generates about 3×10^{11} pixels per night per telescope. An array equivalent in *etendue* to the DMT ($\simeq$ 30 telescopes) would generate $\sim$ 10 terapixels ($\sim$ 20 terabytes) per night, and the 4-telescope POI would generate $\sim$ 2.5Tb per night. Nonetheless, the computer hardware required to process the data from such a system is not overwhelming.

We envisage that the system would generate high S/N cumulative images - these would be averaged on a range of time-scales from individual observing runs to the full duration of the project. Detection of NEO's and transients would involve the following steps:

1. Read-out of a new set of images.
2. Flat-fielding and sky subtraction.
3. Object finding to generate a catalogue of reference stars
4. Astrometric solution by matching stars with those from the accumulated image/catalog database.
5. Modeling of, and convolution with, the PSF.
6. Warping of the image onto sky coordinate system.
7. Averaging new images with cosmic ray rejection.
8. Generating a PSF matched version of the accumulated image.
9. Subtraction to obtain the difference image.
10. Transient/moving object detection.
11. Accumulation of the new contribution to the static sky image.

While somewhat involved, this is no more sophisticated than the type of processing of large mosaic images now commonly performed for purposes such as weak lensing and supernovae searches. The details are discussed further below.

The most computationally intensive steps are the image warping and spatial filtering required for steps 2, 4, 5, 7. Flat-fielding and warping a 2K $\times$ 2K image takes about 7s on a low end 440MHz workstation, and spatial filtering with FFT takes a similar time, so the total processing steps outlined above would take about 40s. Such a machine can process $\sim 10^{10}$ pixels per day and a 4 telescope array would then require $\sim$ 120 such workstations (note that this data reduction is an intrinsically parallel process — see figure 4). However, machines of this class currently cost around \$1K, yielding a total computer cost $\sim$ \$0.12M, and the prices

are falling all the time. Equivalently, a single telescope requires ~ 30 of these workstations, so the cost of computers would be around \$30K per telescope, and negligible compared to the cost of the telescope and/or detectors. These are fairly rough estimates of the minimum hardware requirements (assuming no further optimization of software), and it is possible that the actual requirements might be say a factor ~ 2 higher if, for example, certain critical parts of the analysis were performed on images re-sampled to a smaller pixel scale for greater precision.

We will also need to store the data as it pours off the detector. A night's worth of data is around 600GB per telescope, but 70GB drives can now be purchased for around \$1.4K, so the cost of temporary disk storage would be about one half of the computer cost and again expected to fall rapidly.

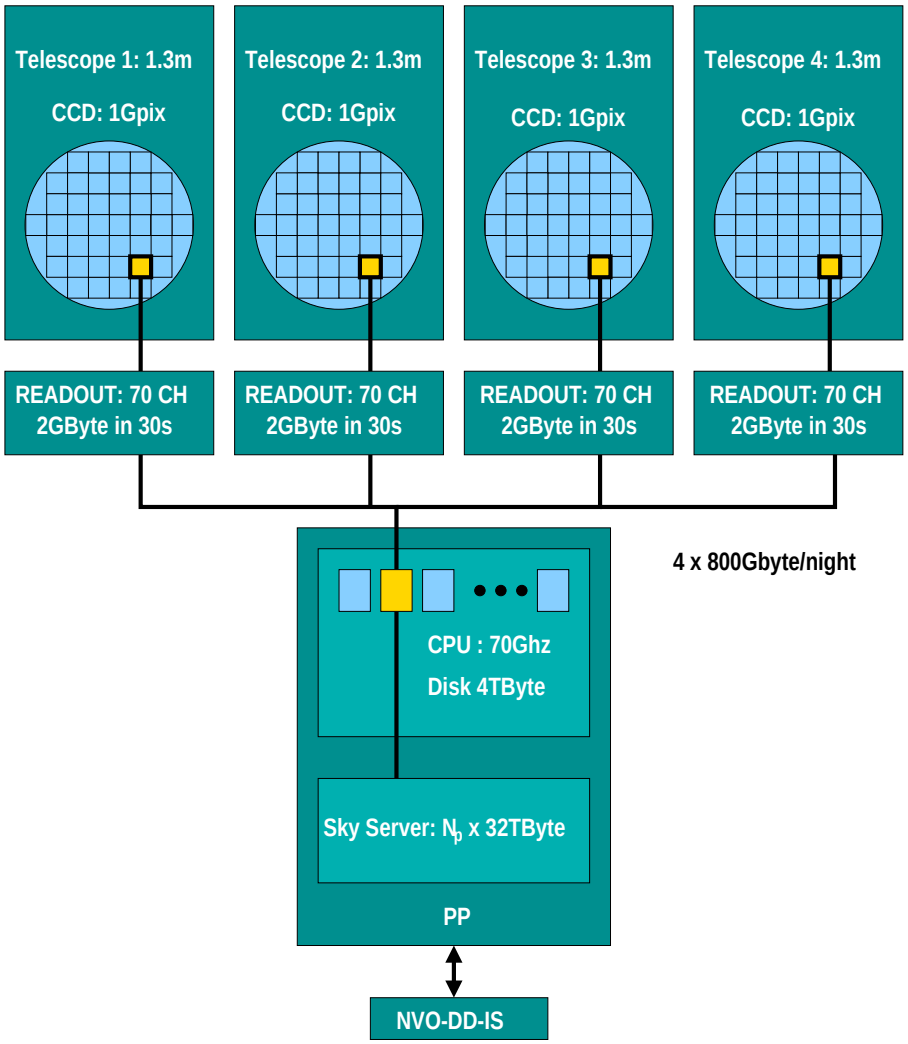

Figure 4: Illustration of the parallelization of the basic data reduction pipeline, here for an array of four telescopes. With the observation strategy envisaged for the POI, the reduction is entirely parallel.

6.4.2 Basic Data Products Storage Requirements

The POI will generate about 2.4TB of data per night, or about 1 petabyte per year. DLT tapes currently cost about \$3 per GB, so the cost of storing all of this would be around \$3M per year. EIDE drives are similar in cost, and SCSI drives are currently about a factor 5 times more expensive. None of these seem attractive options. We propose instead to store only cumulative images, and catalogues of objects and deviant pixels for the individual exposures. We would certainly want to keep on-line the full cumulative image as this will give the highest S/N image to subtract from the new images for transient and NEO detection. If we sample at 0".15 pitch (i.e. a factor 2 finer than the physical 0".3 pixel scale) then the full $28,000\text{deg}^2$ region would occupy about 32TB per passband uncompressed. These images can be compressed by a factor $\sim 2.5 - 3$, so with say 3 passbands, and allowing for some extra calibration images (exposure maps etc) we need $\sim 50 - 70$TB of disk. At current prices this would cost somewhere between $\sim$ \$200K $-$ \$1M (for EIDE or SCSI respectively). This is not excessive. Extrapolating from the present one would expect perhaps a factor 3 fall in prices over the construction time for the project, so the cost of maintaining the cumulative image database is likely to be a similar to the operating costs. There will likely also be further technological advances driven by HDTV which can reduce costs further.

Other data products useful for time varying object detection would be transient catalogs and postage stamps, and lists of pixels differing my more than say 3-sigma from the cumulative image. These could also be kept at little extra cost. In addition, the cumulative images would be saved to tape at intervals.

Access to limited selections of the data products can most easily be provided on the web in a manner similar to the digitized sky survey and USNOA catalogs (where the user simply fills in a form requesting data for a given patch of sky). Large data requests could be filled by mailing tapes. More sophisticated data mining will be accomplished via the NVO (see below).

6.4.3 Software and Data Management Costs

Experience from recent projects such as the MACHO project and the SDSS has shown that software development can be a major component of the cost; comparable to, or even greater than, the cost of hardware. However, these projects created the necessary pipelines essentially from scratch, and were somewhat all encompassing, addressing challenging database problems that will in future be the responsibility of the NVO.

In our case the costs of implementing the basic reduction pipeline are minor since essentially all of the needed software already exists. For example, Kaiser's IMCAT software provides an extensive collection of efficient low-level tools which has been used to implement a very flexible processing pipeline. Since these low level tools are mostly filters which read and write FITS images and/or catalogs via their standard I/O streams, it is also very easy to incorporate external algorithms into the pipeline. The processing required here differs mainly in scale from what we are already doing with large detectors on CFH and on SUBARU, and our pipeline already operates over a parallel virtual machine. There is also a great deal more expertise in this area in Hawaii. Tonry has a similar pipeline for supernova detection; Jewitt has pipelined CFH12K data for KBO searches and finally, there is the Elixir project at CFHT which is now performing all of the basic data reduction (to the point of fully calibrated images) on all of the queue scheduled CFH12K data.

It must be recognized that none of these pipelines are currently automated to the extent that one can simply feed in a stack of tapes and come back later to get fully reduced data. Rather there are certain steps in the process where some kind of human intervention is necessary for the purposes of quality control. However, these steps tend to be associated mainly with *calibration* issues. For example, since flat field images get applied to all of the data, it is worthwhile inspecting the input images to weed out flaws. Similarly, for the astrometric calibration it pays to carefully filter the stars to weed out bad objects. Once the calibration is done, however, the processing of the actual science data continues very smoothly and largely without human intervention. Since the photometric calibration scales with the number of pixels in the camera — which are here about one order of magnitude greater than the CFHT12K for example — this should not be overly demanding, and indeed even these steps could be streamlined further with some effort.

The basic reduction pipeline will therefore be constructed from some combination of these ready made 'in house' reduction packages. Some work will be involved in making these items mutually compatible, and there will also be the job of making the output data streams compatible with the NVO, but these are relatively minor compared to the investment already made in the existing software. Some resources could also be devoted to optimization of some of the critical points in the existing pipe-line, but given the low present cost of computing hardware this should again be a limited undertaking. In addition to pooling the best features from the in house software, we will hope to to build on the experience and manpower from projects such as SDSS, 2MASS, Terapix etc. by co-opting e.g. post-doctoral fellows and perhaps software engineers from these projects.

The scale of the POI project is much larger than e.g. the weak lensing or supernova surveys carried out here. Such projects are executed by very small groups, with the management performed by the PI. This is efficient, but unfortunately does not scale to a project of the size of POI. In order to maintain efficiency and to stop costs spiraling out of control, it is highly desirable to break the data processing management problem up into chunks such that a single person be fully responsible for each component. The various parts of the data management problem include

- Scheduling of observations.
- Running the pipeline reduction.
- Maintaining the pipeline hardware.
- Photometric calibration.
- Astrometric calibration.
- Maintaining the cumulative image data-base and associated hardware.
- Coordinating communication with internal and external scientists and the NVO.

In addition, it would be valuable to have a team member assigned to quality control and to oversee security of the system. Note that some of these tasks — such as the calibration — will tend to be most demanding of resources in the very early stages of the project and will later ramp down. Others — such as maintaining the image database hardware — will tend to ramp up. Not all of the tasks above require a full time employee, so it is reasonable that the total manpower requirement be on the order of 5 FTEs (not all of whom should be PhDs).

6.5 Operation and Maintenance Costs

Operation costs for conventional multi-purpose observatories can be quite high. Here we are considering a specialized, single function instrument, so there are no instrument changes. The telescopes will also be largely robotically operated, resulting in further savings.

IfA staff have considerable experience in running the UH88" telescope, and recently have performed a major upgrade of the telescope control system. Based on these experiences, the UH88" management have made a fairly detailed analysis of the manpower requirements for the POI. As with the data processing, there will be some extra burden as the project gets started, but once the system is working the operating costs are expected to be on the order of $0.4M per year.

6.6 CCD and Camera Development

The main design and development work in this project is associated with the CCDs and read-out electronics. However, this project is by no means alone in pushing these developments, and we anticipate that much of this development work will push ahead on the time-scale for construction of the pilot-project.

- The LBL depleted CCD project is being driven by the requirements of the SNAP-SAT proposal. This has very similar requirements to our wide-field imager in terms of pixel size and physical resolution.
- There is a new Lincoln Labs development emerging, being coordinated by Tonry, to supply very large scale detectors to e.g. the WIYN observatory. These devices will have 12μm pixels and will very likely feature orthogonal charge transfer and wafer-scale integration, both of which are desirable (though not essential) properties for this project.
- Various groups (LBL, Beletic at Keck) are working on developing better, faster cheaper read-out electronics, and the IfA has expertise in this area through the development of read-out electronics for the IR detectors.

It will be necessary to work closely with these groups to obtain design details, prototype devices and to determine the optimal solution.

Design and integration of components into a camera are more project specific and it will be necessary either to hire a specialist or contract the work out to a company such as GL Scientific. This venture could operate under the auspices of the planned Advanced Technology Center.

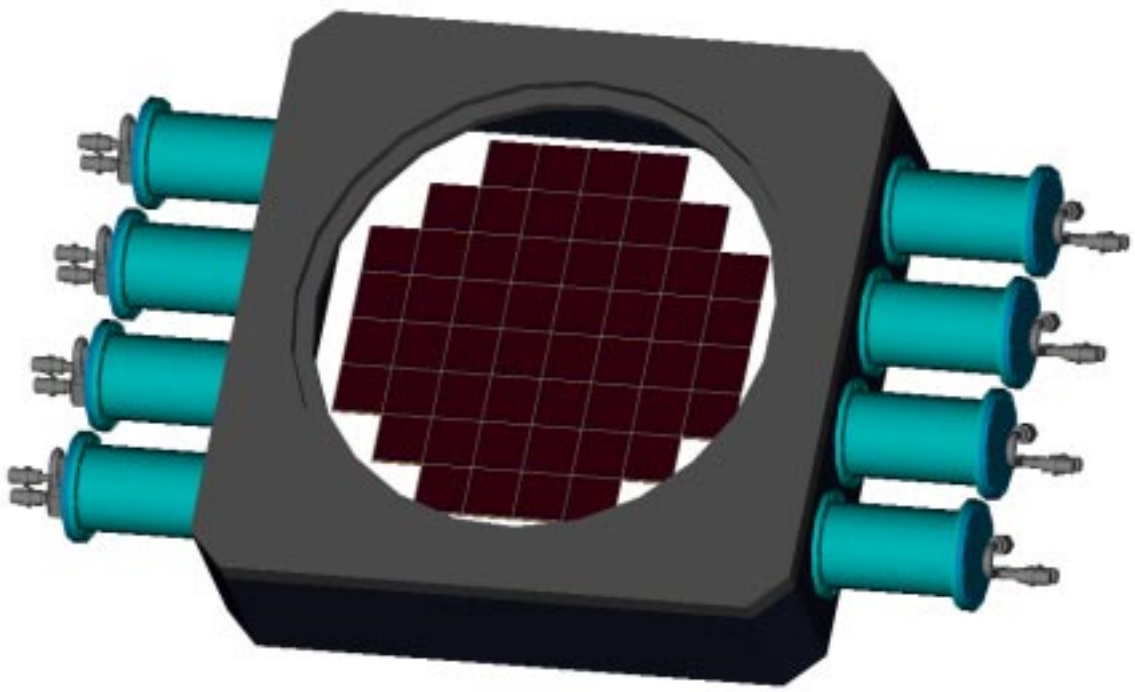

Figure 5: Schematic design for the CCD camera for the POI. Each 5cm $\times$ 5cm block of the array here is in fact an 8×8 array of 512×512 pixel subunits. These are OTCCDs with 12μm pixel size. The camera is cryogenically cooled.

A Economics of Telescope Costs

In the WFHRI proposal, the size of the telescopes ($D \simeq 1.5$m) is dictated by matching the adaptive optics system to the atmospheric seeing. Here we ask: What is the optimal telescope size for ground based large-scale surveys which accept the natural seeing? As already mentioned, without adaptive optics there is no advantage *per se* in having a single large aperture, rather than several smaller ones, provided only that the aperture is sufficiently large that the image size is atmospheric seeing rather than diffraction limited[5]. We are also assuming here that the noise in the images is determined by photon counting statistics rather than by read noise — we justify these assumptions later.

The answer to this question involves a play-off between telescope costs and detector costs. In the limit that detector costs are negligible — a good approximation for very large telescopes and for optical detectors — cost considerations clearly favor small telescopes. This is for two reasons: First, engineering considerations dictate that telescope total system cost must increase at least as fast as the collecting area. It is often said that the cost scales as some power of aperture $C \propto D^\alpha$ with $\alpha \simeq 2.6 - 3$. This is an over-simplification, and there are other factors such as the focal ratio that strongly influence cost, but the conclusion that $\alpha > 2$ seems unavoidable on very general grounds. For example, a 1m mirror which is a few inches thick is effectively rigid, and needs only a simple support. One cannot simply increase the area of the mirror keeping the thickness fixed as the mirror would no longer be rigid. Scaling up rigid designs requires massive mirrors (with cost scaling more like D^3) and the extra weight feeds through into huge increases in the cost of the mount. Most recent large telescope designers have opted instead for segmented or 'meniscus' mirrors. For the former at least, the cost of the mirror surface scales in proportion to the area, but one then needs active mirror control, which adds to the system cost. There is then the problem of supporting the telescope; the wind loading forces increase with area and the mount must still be able to support itself. Similar considerations apply to dome costs, which also increase faster than the collecting area. For small telescopes they are very small. These are the same basic problems of materials science that Nature faces in designing large mammals and are unavoidable. There are also other cost factors which are harder to quantify but still need to be included in a proper cost-benefit analysis. For example, the environmental and political costs to exceed the height of current domes on Mauna-Kea are effectively infinite. Small telescopes may be housed in a low profile building with considerably less environmental impact.

The second reason is related to the first in that to avoid punishing dome costs, large telescope designers have been inevitably led to compact, and therefore optically fast, designs. For example, the current 8-10m class telescopes have domes very similar in size to that of the slower 3.6m CFHT or the AAT. However, fast design and wide field of view tend, on general optical principles, to be incompatible. For a given *class* of design (ie a specific combination of mirrors, lenses) the FOV tends to be an increasing function of the focal ratio, so the faster the design the smaller the FOV. Now one can increase the FOV for a given focal ratio by going to a more complicated class of design with more mirrors and lenses but there is a significant penalty for this, not just in the cost of manufacturing more mirrors and lenses, but also in reflection losses and chromatic aberrations etc. There are also possible difficulties in aligning and/or actively

[5]In fact, there is some advantage in using *small* telescopes in this regard since one can 'guide out' some of the effect of low level 'planetary boundary layer' turbulence (see §D) and thereby sharpen up the image as compared with a large telescope.

controlling a complex system with many large elements. The DMT design is able to produce good images over a 3° degree field with an $f/1.25$ focus, but to do this it requires three mirrors, two lenses and a curved focal plane — a total of six deformations of the wavefront — and there is quite large obstruction of the 8.4m primary. By contrast, the 40″ $f/7$ at Las Campanas achieves the same FOV with two mirrors plus a single corrector and no focal plane curvature (Bowen & Vaughan 1973), and this simple design delivers excellent image quality. 'Astrograph' telescopes achieve even wider fields of view with very simple Newtonian + refractive corrector optics, but are quite slow. The Schmidt camera, and its all reflective analogue the Couder telescope (Willstrop 1983), have very wide fields of view, but are again necessarily very long, and so are impractical for large apertures. For small telescopes, and particularly for close packed arrays thereof, the enclosure cost penalty for slow and/or long designs is small — if one were to bundle a bunch of Couders or Schmidt Cameras together they would be no longer than a single large aperture telescope.

The three-mirror designs offer quite a jump in compactness as compared to the Schmidt and Couder, but as a class they still reveal the antagonism between speed and field of view. Willstrop's Mersenne-Schmidt design is a $f/1.6$ and offers a 4deg diameter FOV as compared to the $f/1.25$ DMT's 3deg. It is, however, 50% longer for given primary aperture; this is a serious handicap for a 8m design, but not for smaller apertures.

To add an empirical datum to the foregoing arguments, we note that the US Naval Observatory recently purchased a $f/4$ 1.3m telescope, with 1°.7 diameter FOV from DFM Engineering[6]. The design (Melsheimer & MacFarlane 2000) is a Ritchey-Chretien with corrector plate similar to, but somewhat faster than, the Bowen-Vaughan Las Campanas 40" design. Such a telescope can be purchased for around \$900K, and the cost per unit collecting area is about $\$0.53\mathrm{M/m^2}$, about a factor 5 less than the DMT. The FOV here is smaller, so the specific telescope cost is $\chi_{\rm tel} \simeq 0.29\$\mathrm{M/m^2/deg^2}$, but this is still considerably better than the DMT, and unit costs for multiple orders would be smaller still. (We will consider detector costs presently).

It is possible to extend the field of view by making the design slower, as in the Las Campanas 40", or adding a second refractive correcting element, as in the SDSS telescope, with little increase in construction cost. Both designs deliver a 3-degree diameter field of view. We have pushed the Bowen-Vaughan design to $f/5.4$ and still obtain very good image quality over the full 3° field ($\Omega \simeq 7\mathrm{deg}^2$) and one of these telescopes with $D = 1.3$m would have $A\Omega \simeq 9.4$, about as powerful as SUBARU/SUPRIME or CFHT/MEGACAM and one third as powerful as VISTA, but clearly much cheaper. With a 3 degree field of view and $C_{\rm tel} = \$900$K the specific telescope cost is $\chi_{\rm tel} \simeq 0.1\$\mathrm{M/m^2/deg^2}$. Vignetting losses of $\sim 25\%$ in the BV design push this up, but discount for multiple orders may offset this.

As a more extreme example consider the 16″ (0.4m) Schmidt-Cassegrain from Meade, which retails for around \$15K, complete with mount and computer control system. The cost per unit area is $C/A \simeq \$95\mathrm{K/m^2}$, about a factor 25 better than the DMT. This nicely illustrates the cost vs area scaling described above combined with the cost benefits from producing multiple units. This delivers $\chi_{\rm tel} \simeq (0.12\mathrm{deg}^2/\Omega)\$\mathrm{M/m^2/deg^2}$ which, in the absence of detector costs, would outperform even the DMT for any $\Omega \gtrsim 0.25\mathrm{deg}^2$. This type of design delivers a very wide field so potentially the specific telescope cost could be very low. An obvious question for such an approach is the cost of detectors. We will consider this in more detail below, but to see

[6] `http://www.dfmengineering.com`

that these are not necessarily overwhelming, we note that Apogee[7] are marketing a complete cooled camera using a 4K $\times$ 4K Kodak detector for $\simeq$ \$30K which, with this telescope, delivers a $\Omega = 0.25\mathrm{deg}^2$ FOV, and this system then has a total specific cost of $\chi_{\mathrm{tot}} \simeq 1.42\$\mathrm{M/m}^2/\mathrm{deg}^2$. This is admittedly not quite as good as the DMT, but is similar to the estimated performance of VISTA, and outperforms all existing wide field imagers on large telescopes by a huge margin. A disadvantage of this system for very good sites like Mauna Kea is that in good seeing the image quality will be compromised by diffraction effects (see §D and figure 9), but for mainland sites, or for applications which do not require superb image quality this is already a viable approach and, as we shall discuss later, there is good reason to think that detector costs can be decreased considerably.

Further gains in cost effectiveness result if we consider performing a large survey with an *array* of small telescopes. An array of 28 $D = 1.3$m 3deg FOV telescopes would have the same collecting area and *etendue* as the DMT. With this level of mass-production there should be considerable economies of scale in many aspects of the manufacturing process, and it may then be worth considering alternative technologies such as light-weight or replicated mirrors, novel mounts etc.

One factor which we have so far ingored is man-power costs for maintainance and telescope operation. In this regard we note that closed cycle coolers which are now becoming commonplace obviate the need for manually attending the detectors. Also, in projects such as TAOS[8], GNAT[9], and the Faulkes telescope (ref...) the telescopes are effectively robotic and the TAOS telescopes have been designed to operate in quite inaccessible locations with only infrequent maintainance.

To summarize, optics and materials science considerations generally tend to favor arrays of small, slow designs for wide field surveys (while there are certainly clever counter-examples like Willstrop's Mersenne-Schmidt, these still appear to be relatively costly). Conventional small telescopes as are readily available from commercial vendors outperform large telescope designs, and for a project of the scale envisaged by the decadal review the possibilites for cost savings from new technology are considerable. however, an obvious missing factor in the above analyis is clearly detectors costs, which we now consider in more detail.

[7] `http://www.apogee-ccd.com`
[8] `http://taos.asiaa.sinica.edu.tw`
[9] `http://www.gnat.org`

B Detector Issues

B.1 Charge-Diffusion

A fundamental limit on small telescope imager designs comes from the finite resolution of the CCD. The pixel size, of course, limits the resolution, but, within reason, can be chosen fairly arbitrarily (note that the $15 - 25\mu$m pixel sizes typical are huge compared the the scale of electronic architectures in computer processors or memory chips). A more critical limit comes from charge diffusion. In a CCD charge carriers are created — for blue light this happens right at the 'back' surface — and then drift towards the gates where they accumulate in the 'egg-crate' pattern potential wells. As they drift they diffuse. This effect is well understood theoretically (Groom et al. 2000; Groom 2000) and results in an essentially Gaussian probability distribution for the lateral displacement. We shall denote the scale length by σ.

The charge diffusion has been measured for some LBL devices[10] at Lick to be $\sigma \simeq 6.5 - 9.5\mu$m for 200μm and 300μm thick devices respectively. These measurements were made at an operating voltage of $V = 40$V. The charge diffusion scale is linearly proportional to the thickness and inversely proportional to $\sqrt{V}$, so the resolution could be improved by operating at higher voltage and perhaps using even thinner chips (though this will incur some decrease in yeild). Note that these measurements were for blue light, which is absorbed almost immediately on entering the device, so this is a worst case and red light would be expected to have a higher resolution. This is convenient, since the natural seeing width also decreases with wavelength. It is not unreasonable to assume that one could obtain a charge diffusion length of $\sim 3\mu$m with a suitable combination of voltage and device thickness (though admittedly this has not yet been demonstrated). This would allow very short focal length designs, with corresponding decrease in telescope costs. More information on the yeild and performance at high operating voltages is needed to determine the optimum choice of parameters.

The charge diffusion scale has been measured indirectly for MIT devices by Cavadore[11] at ESO. He shone a small spot of light on the center of a pixel and measured the fraction of electrons collected within that pixel — this is the Strehl ratio — and obtained values ranging from $\sim 80\%$ in the red to $\sim 50\%$ in the blue. Comparing with the upper panel in figure 6 shows that this corresponds to $\sigma \simeq 4.5 - 7\mu$m respectively.

The effect of charge diffusion on the MTF for Loral and Tek chips has been measured by Andersen and Sorensen[12] at IJAF. Their measurements correspond to huge values of $\sigma \sim 16\mu$m for the Loral devices and only slightly better for the Tek devices. The reason for this surprising result is unclear.

We have measured the charge diffusion for an MIT 40μm device using a pin-hole mask kindly supplied by Steve Holland. For the smaller holes we found very high ($\gtrsim 80\%$) central pixel fraction, corresponding to a charge-diffusion scale $\sigma \simeq 4.5\mu$m.

The charge diffusion scale is an important factor in designing small telescopes, as the requirement that charge diffusion not degrade the image quality sets a limit on the plate-scale. The diminution of the maximum of the PSF is shown in figure 6 as a function of the angle corresponding to σ in units of the FWHM of the natural atmospheric PSF. If we require that the width of the PSF be degraded by less than 10% then we require that $\sigma \leq 0.21\times$ FWHM.

[10] `http://snap.lbl.gov/pubdocs`

[11] `http://www.eso.org/ ccavador/CCDtests/MIT`

[12] `http://www.astro.ku.dk/ ijaf/mtf/mtf.html`

For FWHM = $0''.6$ and a physical diffusion scale of $\sigma = 3\mu$m this implies a plate scale of $s \simeq 24\mu$m/arcsec. The nominal design for POI has a plate scale of 34μm/arcsec which would be compatible with a gaussian diffusion scale $\sigma \simeq 4.5\mu$m.

B.2 CCD Costs

B.2.1 MIT/Lincoln Labs Devices

The cost of the MIT/Lincoln Labs 2K $\times$ 4K thinned CCDs as supplied to the DEIMOS project for example was around \$24K per chip. What is most relevant here is the cost per unit area, which was around $c_{\rm CCD} \simeq$ \$1.3K/cm^2 or \$13M/m^2, and would result in specific CCD cost of $\chi_{\rm CCD} \simeq 5.1 \times 10^{-3} F^2$\$M/m^2/deg^2. For an $f/4$ design this is $\chi_{\rm CCD} \simeq 0.08$\$M/m^2/deg^2 and comparable to the telescope specific cost for a 1.3m design with a 3deg diameter FOV of $\chi_{\rm tel} \simeq 0.1$\$M/m^2/deg^2.

It may be possible to do better than this as the following numbers show. The cost of a run of 12 x 150mm diameter wafers from Lincoln Labs is $\simeq$ \$400K, including the cost of thinning. The total area is 0.21m^2, giving raw cost of $c_{\rm CCD} \simeq 1.9$\$M/m^2, smaller than the actual cost by about a factor 6. What accounts for this? First, there are costs involved in cutting up the wafers, mounting them and making connections, applying AR coatings, and testing, but these are fairly minor. The major factors are first that with large rectangular devices on circular wafers, the fractional area used is only about 60%, and second that the yield is rather low as there are failures both in fabrication and in thinning. If only 25% of the devices are of science grade then the costs are increased by a factor $1/(0.25 \times 0.6) \simeq 6$ which accounts for the discrepancy between raw and actual costs.

The failure rate due to random shorts is $\simeq$ 30%, and the area utilization for these large rectangular detectors is $\simeq$ 60%. With smaller individual units both of these factors could be increased to say $\simeq$ 90% and this would result in roughly a factor two increase in the effective yield. One attractive possibility is to make large wafer-sized units consisting of a large number of small 'cells' ganged together, and accept a small fraction of dead cells. It is very hard to see why this should a problem; dead detector cells will get moved around as one dithers, so these dead regions will get filled in even in a single telescope instrument, and for an array the effect of dead cells would be negligible. Incorporating this factor 2 gives a cost per unit area

$$c_{\rm CCD} \equiv \frac{C_{\rm CCD}}{A_{\rm CCD}} \simeq \$6{\rm M/m}^2 \tag{9}$$

and specific CCD cost

$$\chi_{\rm CCD} \simeq 0.037\eta^{-1}(F/4)^2 \$ {\rm M/m}^2/{\rm deg}^2 \tag{10}$$

which is the value we shall adopt in the main text. We believe this is a fairly conservative number, as it is firmly based on real costs of actual devices. The main uncertainty here is whether it will be possible to increase the yield in the thinning process.

B.2.2 Depleted DDCs

A recent development that could result in large savings is the fully depleted devices developed by the LBL group. These are not thinned, and they estimate that the cost for a run of 20 $6''$ diameter wafers is around $\sim$ \$100K giving a or raw cost per unit area of ~ 0.3\$M/m^2. Even for

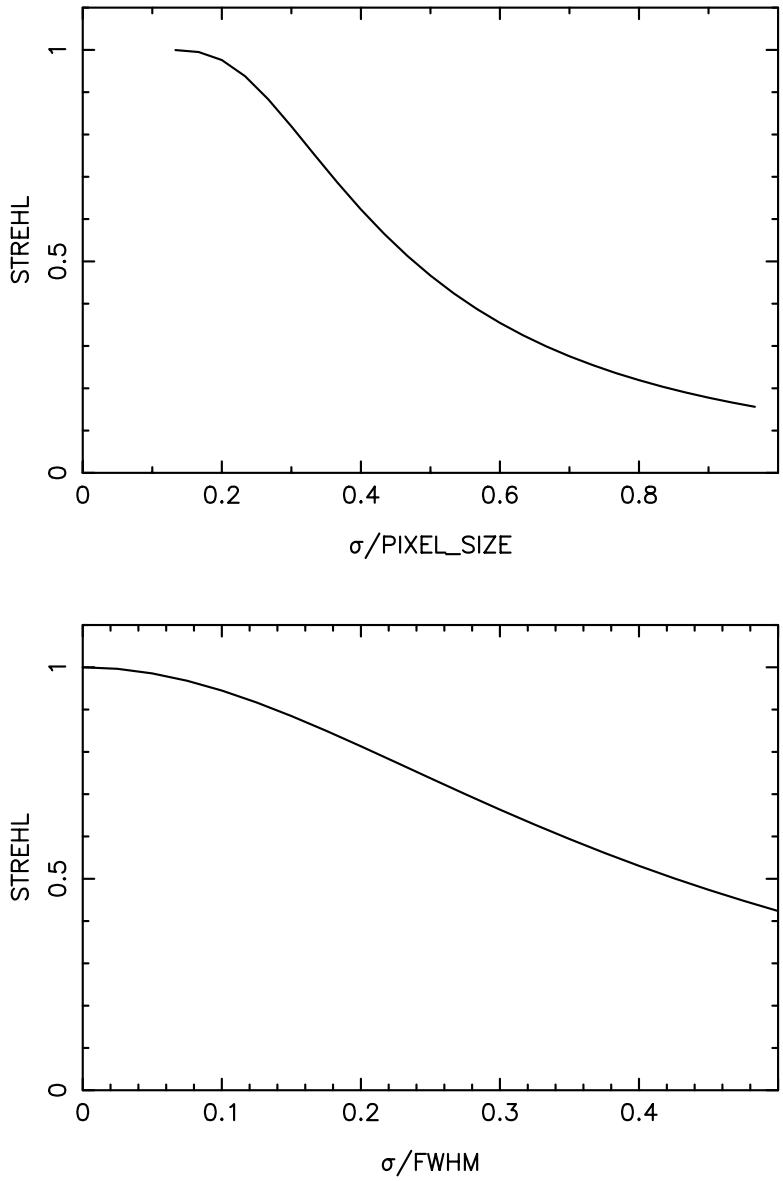

Figure 6: Effect of charge diffusion. The upper panel shows the effect of charge diffusion on the Strehl ratio in the absence of seeing, pupil effects. This can be used to convert Cavadore's Strehl ratio measurment to a σ value. The ordinate in the lower panel is the normalized Strehl ratio (i.e. the peak of the PSF) for atmospheric seeing convolved with a Gaussian of width σ. This figure shows that the Strehl is reduced by $\simeq$ 20% when the Gaussian diffusion scale is about 0.21 times the FWHM of the seeing disk. This criterion corresponds to an increase in the seeing width of about 10%.

large rectangular devices (60% area utilization) and assuming 25% yield the cost per unit area is $c_{\rm CCD} \simeq 2.0\$\mathrm{M/m^2}$ and specific CCD cost is then $\chi_{\rm CCD} \simeq 1.65 \times 10^{-2}\eta^{-1}(F/4.5)^2\$\mathrm{M/m^2/deg^2}$, and as before, the yield could probably be increased by a factor 2 by using smaller individual units. At this price level the CCD costs are almost negligible as compared to the specific telescope cost for the kind of design considered here, and it may be worth considering more carefully even slower designs, or Schmidt cameras, with even larger fields of view.

The LBL detector project is being driven largely by the SNAP-SAT project which has very similar requirement — cost, small pixels etc – as the project proposed here.

LBL are exploring licensing agreement with commercial vendor. Hamamatsu are also said to be interested in developing depleted CCDs.

B.2.3 IR Detectors

The foregoing numbers apply only to optical detectors. Infra-Red detectors are currently a lot more expensive than optical CCDs, and this is bad for small telescopes. Currently IR detectors like the HAWAII-2 array cost about 8 cents a pixel whereas the 10μm pixels assumed here cost around 0.05 cents per pixel. However, there is rapid progress and the costs are likely to fall quite fast.

B.3 Dewar, Cooler and Shutter

Cameras on the scale considered here could be cooled with a few 'cryotiger' (ref ....) closed cycle coolers costing approximately \$8K a piece. There is also the cost for the container, shutter, and, if required, a filter wheel. In many cameras these are quite expensive but this mostly reflects the large design costs for one-off projects. For an array, these costs would be spread over multiple units. Camera manufacturing is now a fairly mature field; the development work is largely done and there is a growing pool of available talent in the community and costs will inevitably fall.

B.4 Read-Out Electronics Costs

The cost of the read-out electronics depends critically on two factors: the speed with which one wishes to read out and the desired read-noise. These are both very strong functions of the integration time; for long integrations one can tolerate long read times and also higher read noise.

Near earth objects searches present the greatest challenge as they move at a rate of $\dot{\theta} \simeq$ 0.3deg per day or about 0.012arcsec/sec and simple signal-to-noise considerations suggest that ideally one would like to take exposures on about the time-scale for the object to move a few resolution elements or about 1 minute for $R \simeq 1$AU. For the fainter objects we will detect the typical angular velocity is still lower.

A single channel capable of reading at a rate of about 125K pixels per second currently costs about \$5K from Leach, and delivers a read noise on the order of 1-3 electron. This is somewhat better than we need, since such searches would be performed with broad band filters (or no filters) and the sky-noise would be on the order of 10 electrons. In what follows we will assume that we can read at a rate of 500K pixels/second without compromising this. If we require that we read out in 1/2 of the integration time (suffering an overhead of 33%) then we would need

about 9.6 channels per square degree (assuming here $0''.3$ pixels). For a 3-degree diameter field ($\Omega = 7.1\mathrm{deg}^2$) this requires $\simeq 70$ channels, with cost on the order of \$340K and specific cost

$$\chi_{\mathrm{elec}} \simeq 0.036\eta^{-1}(D/1.3\mathrm{m})^{-2}\$\mathrm{M/m}^2/\mathrm{deg}^2. \tag{11}$$

As with the estimate for the CCD costs, this is a conservative estimate as it is the cost for 'off-the-shelf' products. It is considerably less than the telescope cost for the design we are considering. For *etendue* $A\Omega \simeq 10\mathrm{m}^2\mathrm{deg}^2$ telescopes (ie equivalent to CFHT/MEGACAM or SUBARU/SUPRIME) the cost would be $C_{\mathrm{elec}} \simeq C_{\mathrm{CCD}} \simeq$ \$350K. This is a non-trivial cost component, but still a small fraction of the total. For other science goals the readout times can be much longer and costs correspondingly lower. It is also an area where one can expect large increases in efficiency. The 'FIERA' systems developed at ESO are said to be superior in performance to the Leach systems and the Keck instrument group under Beletic are also developing advanced read-out electronics. LBL are developing ASICs for the read-out electronics for the SNAP-SAT camera. Another interesting approach is Tonry's 'hybrid' detector scheme but this require some R+D. Thus we consider (11) to be an upper limit, and that if one or other of the projects mentioned above come to fruition this cost component could be reduced considerably.

C Sensitivity and Dynamic Range

In this appendix we estimate exposure times and sensitivity. We compute 'trailing losses', estimate read noise and discuss dynamic range, cosmic ray rejection and the possibility of drift-scan operation.

C.1 Exposure Time Calculations

In the imcat object detection algorithm (and presumably in other efficient algorithms) sources are detected by convolving the image with a kernel. For point source detection the optimum kernel is just the PSF, which we will denote by $g(\mathbf{x})$. If the electron count per second from the source is $N_{\rm obj}$ and the electron count per second per unit solid angle from the sky background is $\overline{n}$ then the squared signal to noise ratio of a detection (which we take to be the height of the peak of the convolved image divided by the rms smoothed sky fluctuation) is

$$\eta^2 \equiv ({\rm S/N})^2 = \frac{N_{\rm obj}^2 t}{\overline{n} \int d^2x \; g^2(\mathbf{x})} \tag{12}$$

where the PSF is normalised such that $\int d^2x \; g(\mathbf{x}) = 1$.

Note that we are trying to detect objects after having subtracted the static sky. This in important since otherwise the clutter of background galaxies — the 'cosmic wallpaper' — will increase the noise.

Computing the PSF assuming Kolmogorov turbulence (and neglecting effect of pixel size, aperture diffraction and guiding effects — a reasonably good approximation here) we find

$$\eta^2 \simeq 0.318 \frac{N_{\rm obj}^2 t}{\overline{n}({\rm FWHM})^2}. \tag{13}$$

(For the commonly used, but qualitatively and quantitatively incorrect, Gaussian model the numerical coefficient is $2\ln(2)/\pi \simeq 0.441$.)

The Decadal Review LSST specification is to be able to detect asteroids to $R = 24$. To estimate the required exposure times we have used the table of observed sky background levels with the CFH12K from Cuillandre's web-page. Assuming $V - R \simeq 0.4$, unit airmass, FWHM= 0.6, and 5-sigma of a point source we find integration times:

$$\begin{aligned} t(R) &= 115{\rm s} \\ t(V) &= 134{\rm s} \\ t(V+R) &= 63{\rm s} \end{aligned} \tag{14}$$

where we have assumed 4×1.3m diameter telescopes with the same percentage obscuration as CFHT. The last figure is the integration time for a broad filter spanning the standard V and R passbands.

There are various minor adjustments that should be made to these numbers

- The measured sky values are $\sim 20\%$ higher than we have measured more recently. This is perhaps a result of varying solar activity. Using our measurements would decrease the required integration times by $\sim 20\%$.

- Trailing losses (see below) for a typical velocity ($\dot{\theta} = 0^\circ.3$/day) increase the integration time by about 20%.
- Our optical design has fewer optical surfaces and therefore somewhat higher throughput than the CFHT.
- The quantum efficiency for the LBL devices is higher than for the CFH12K devices.
- The integration times for finite zenith distance will be increased largely because of the poorer seeing (the FWHM is expected to scale as the 3/5 power of the airmass and consequently integration times scale as the 6/5 power). There is also a further increase due to the increase in the sky brighness, but this is a relatively minor effect. The measured median seeing at CFHT (averaged over a range of airmass similar to what our survey will have) is around $0''.7$. It is reasonable to assume that we will have slightly better median seeing than this (see §D).

As these are pretty much balanced between positive and negative corrections, the above figures are probably fairly accurate.

C.2 Trailing Losses

Sensitivity to moving point sources is reduced if they move appreciably during the integration. The effect on the squared signal to noise ratio is shown in figure 7. For example, if the object moves the FWHM during one integration time the squared signal to noise is reduced by $\simeq 0.84$ compared to a stationary source, thus requiring a 19% increase in integration time.

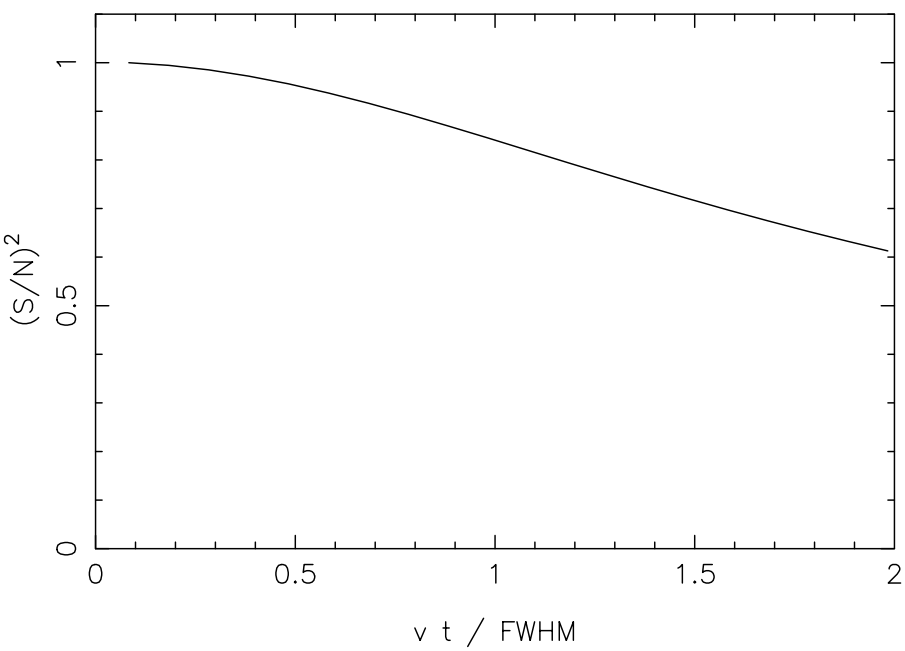

Figure 7: Trailing losses for moving point sources and assuming Kolmogorov PSF.

These numbers suggest that an integration time of say 60s is reasonable from the point of view of avoiding large trailing losses. Now there are certainly some objects which will be

moving much faster than we have assumed, and for them the trailing loss will be more severe (limiting flux proportional to sqrt(angular velocity)) but this is not really a problem. Fast movers are necessarily very close to us, so if they're anywhere near our detection limit they are necessarily of very low mass and hence not dangerous. Put another way, if our goal is to detect all the objects of size > 300m say then they will either be detected when they are far away (and therefore faint and slow) or nearby (and therefore bright and fast).

C.3 Read-Noise

The above calculation neglects the effect of read noise. With $D = 1.3$m and $\theta_{\rm pix} = 0''.3$, and scaling from the CFHT measurements, the $V + R$-band dark sky gives $\simeq 3.6e$/pixel/s, so with read noise of a few electrons the images will be sky-noise dominated for any exposure time $\gg 1$s, so read-noise should not be a problem for any reasonable exposure times.

C.4 Dynamic Range

The rate at which photons are collected per pixel is proportional to $D^2\theta_{\rm pix}^2$. If we assume that the 'full-well' capacity of a pixel is proportional to $d_{\rm pix}^2$ then a pixel will saturate after integration time

$$t_{\rm max} \propto \frac{d_{\rm pix}^2}{D^2\theta_{\rm pix}^2} \propto F^2 \tag{15}$$

so the slower the optical design, the longer it takes to saturate a pixel.

Saturation limits the *dynamic range* of images. The dynamic range for small telescopes is greater than for a single large telescope.

C.5 Cosmic Ray Rejection

As above, the number of sky photons collected per unit time scales as $D^2\theta_{\rm pix}^2$, while the number of cosmic rays scales as the pixel area $d_{\rm pix}^2$, so cosmic rays are relatively more of a problem in a single image from a small slow-beam telescope than for a large one. However, for an array of telescopes one has more images to average over, and so cosmic ray rejection is therefore easier for an array of small telescopes.

Simultaneous observations with an array of telescopes offer a big advantage for NEO detection. Compare say a 6-sigma detection in a single image taken with a 2m telescope and a 6-sigma detection in an image formed by summing four images from four 1m telescopes. In the former case one has essentially no idea whether the object is real or a cosmic ray, while in the latter, if the object is a cosmic-ray or similar artefact then it will appear in just one contributing image, and at the 12-sigma level and will be easily recognizable.

C.6 Drift-Scan Operation?

Many wide field surveys employ some kind of drift scan mode. Sidereal scanning would certainly reduce the cost of the telescopes. However, in the present application we have very wide fields and we are intending to obtain very good image quality; this makes drift scanning very hard, and we do not intend to employ it.

D Finite Aperture Effects

D.1 Diffraction Limit

For sufficiently small apertures, diffraction effects become important and degrade the image quality. This is illustrated in figure 8 and 9 which show the FWHM and the profile of the PSF computed for 0".6 natural seeing and for various apertures. These figures show that for $D \gtrsim 1$m and at optical wavelengths diffraction effects are very small.

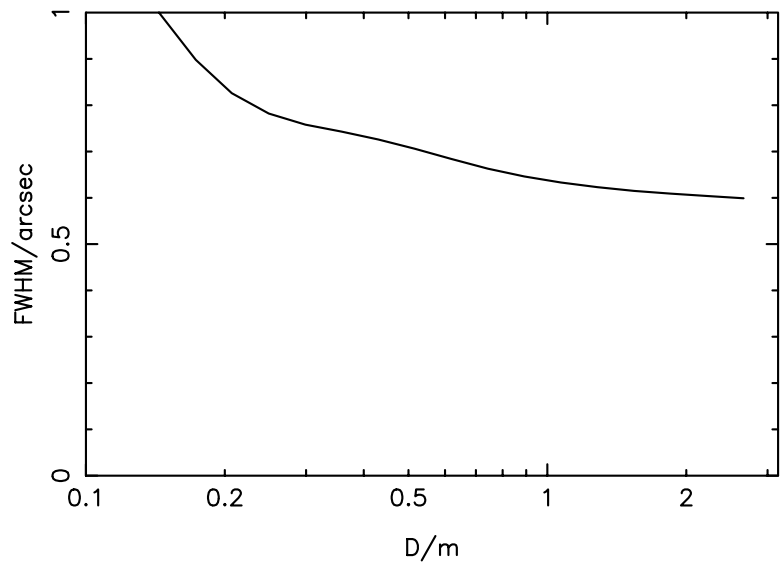

Figure 8: FWHM of the PSF versus aperture size for $0''.6$ natural seeing and for $\lambda = 0.6\mu$m.

D.2 Fast Guiding

These calculations do not include the effects of guiding — it is assumed that the telescope is simply tracking perfectly. With guiding, however, the performance could be considerably better, and small telescopes should outperform large telescopes. The reasoning behind this is that analyis of SCIDAR observations (Racine 1996) indicates that the median seeing in the I-band say should be around $0''.4$, while measurements at CFHT[13] for example show that this is extremely rarely achieved (though SUBARU may be doing better than other facilities), and that a median value of $\simeq 0''.7$ is more appropriate. This suggests that most observations are not limited by the 'free-atmosphere' seeing, but by a combination of low-altitude turbulence, dome seeing and wind-shake or other imperfections associated with the telescope control. With a small telescope, all of these effects can be ameliorated, simply by guiding well. If we assume that the low level effects are due to turbulence, then guiding will give a total PSF which is like that computed in by Kaiser, Tonry, & Luppino (2000), but then convolved with the seeing disk for the free atmosphere effects. We have made detailed calculations of this (see figure 10) and find that it is quite reasonable to expect to achieve FWHM below $0''.5$ a good fraction of the time. For this to work best, it is necessary to monitor the motion of several guide stars across the field. With a single guide star there is the problem that one does not want to guide out

[13] `http://www.cfht.hawaii.edu/Instruments/Queue`

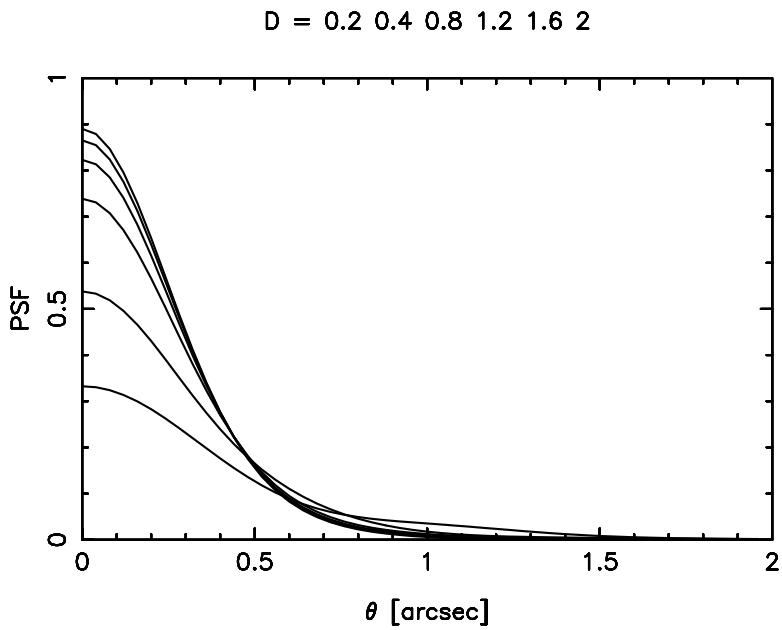

Figure 9: Profile of the PSF versus aperture size for $0''.6$ natural seeing and for $\lambda = 0.6\mu$m.

the effect due to the upper atmosphere as this has a small isoplanatic angle. Now the different layers tend to have quite different time-scales, with the low level turbulence being much slower, so one can filter out the high frequency high-altitude effects to some extent, but averaging over a number of widely separated stars is preferable. The number density of sufficiently bright stars ($\sim$ 16th magnitude) is on the order of a hundred per square degree, so if we cover say 5% of the focal plane with small devices to be used for monitoring guide stars then the averaging will isolate the low level turbulence effects.

It is possible, of course that some of this 'excess seeing' is due to wind-shake (i.e. telescope oscillations excited by wind buffeting). If this is simply rigid motion of the whole system then proper guiding should remove this completely, regardless of the size of the telescope. However, with a large telescope it is entirely possible that higher order modes are excited (e.g. 'pringle' like oscillations of the primary) which would not be taken out by guiding. For small telescopes with rigid primaries one can be confident that these higher order modes will be absent, so, much as with turbulence, there is a clear advantage to small apertures.

D.3 Higher Order Correction

As we have discussed, for a $\sim \$100 - 200$M scale project like the LSST concept, it would make sense to consider actively controlled light-weight or replicated mirrors (this is *not* a viable option for the phase-A study). This opens up additional interesting ways to deal with the low level turbulence. If the telescopes are equipped with a few small telescopes which measure the wavefront tilt around the perimeter then this provides enough information to take out essentially *all* of the low level phase fluctuations, and the images would then be solely limited by the free atmosphere, with median FWHM $\simeq 0''.4$ and with a broad approximately log-normal distribution, so much of the time the image quality would be very good indeed. There is still some uncertainty in the statistics of the low versus upper atmosphere, and the relative role of

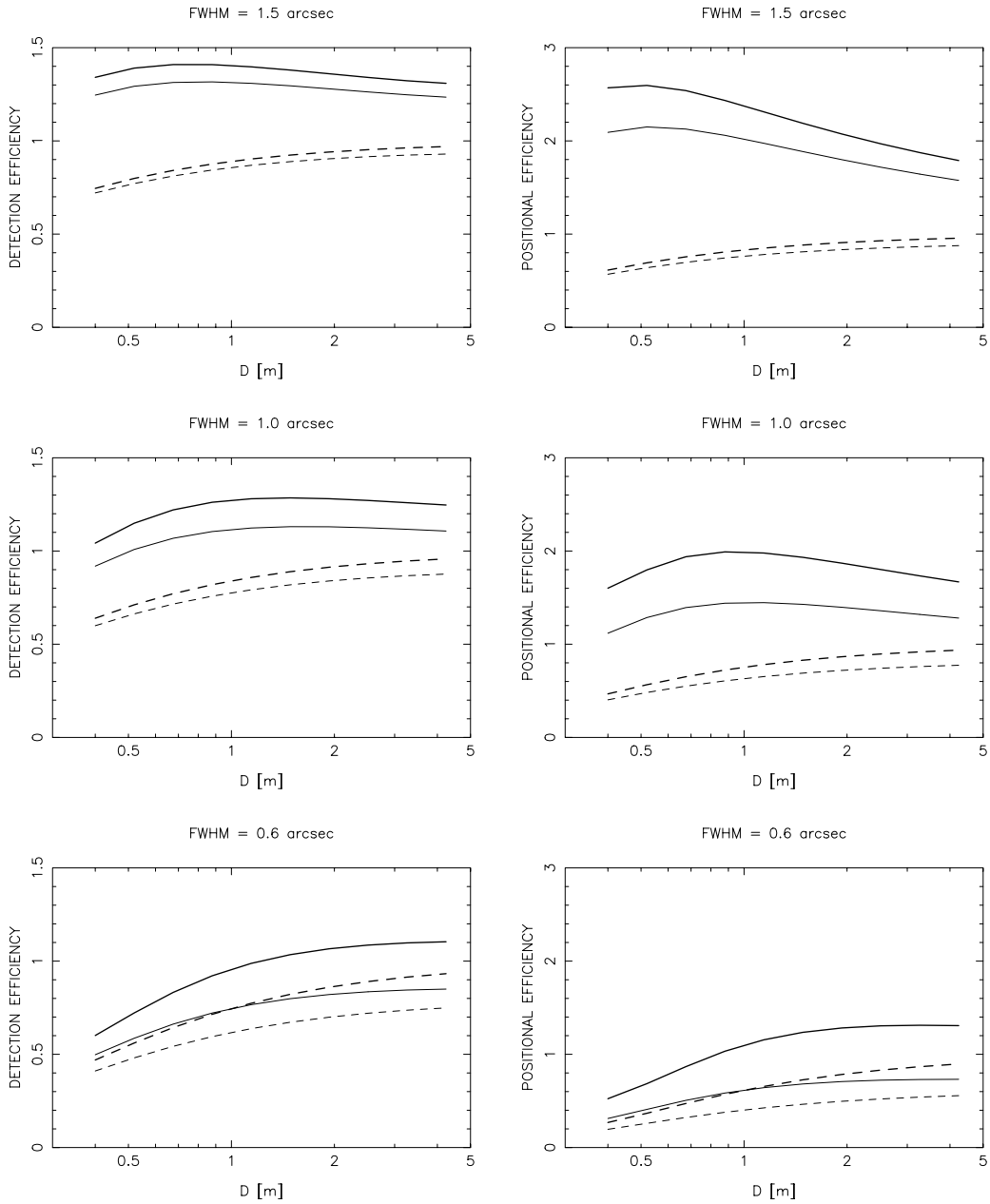

Figure 10: These plots show how the system efficiency depends on the aperture size. Efficiency is measured relative to the efficiency (per unit area) of a hypothetical infinitely large telescope which accepts the natural seeing. Panels on the left show the efficiency for object detection: $\int d^2z\ \tilde{g}^2(z)$ and on the right for object position: $\int d^2z\ z^2\tilde{g}^2(z)$. In each case we have assumed 'free-atmosphere' seeing of FWHM $0''.4$ with an additional boundary layer component to give total seeing FWHM as indicated. The dashed lines are for no fast guiding and the solid lines show the effect of centroid guiding to ameliorate the boundary layer seeing (assumed to have a large isoplanatic angle). For each pair of lines, the heavy line assumes perfect chip resolution while the lighter line shows includes a Gaussian component to the PSF with scale-length $\sim 0''.13$. This corresponds to a charge-diffusion scale length of 4.5μm in a 7m focal length system.

turbulence and other effects, but these can be resolved by the pilot project.

E Temporal Sampling

For long, or *cumulative*, integrations of the static sky the science output is proportional to the product of the collecting area and the solid angle. For transients, the figure of merit is different, and this may also influence the design choice.

Now an array can always be operated in a mode where all the telescopes point at the same field, in which case the performance in regard to transient events is the same as for a single telescope with the same collecting area. Strictly speaking, this is true provided the integrations are long enough that the images are sky noise, rather than read noise, dominated, but for any reasonable integration times this is not an issue. An array can therefore never perform *worse* than a single large telescope, but it can also scan a larger swath of sky, though of course to a shallower depth for given integration time. For some applications this conveys a distinct advantage. For example, if there is a population of rare transient objects with power law flux distribution $N(> F) \propto F^{-\alpha}$ then if $\alpha > 2$ the best strategy is to go deep and point all the telescopes at a single patch, but if $\alpha < 2$ the detection rate is increased by surveying a larger solid angle less deeply.

Most populations of astronomical objects have $\alpha < 2$, for well understood reasons: The 'natural' value for α is the Euclidian value $\alpha = 3/2$, which is that seen by an observer embedded in a uniform sea of objects. This would be appropriate for an observer embedded in a locally uniform cloud of sources and for flux levels such that one cannot see to the edge of the system. At fainter flux levels the finite size of the system (for the solar system, galactic halo etc) or, in a cosmological context the $(1+z)^4$ dimming, means that the slope of the flux distribution will inevitably shift to $\alpha < 3/2$.

A powerful mode of operation for transient searches for short time-scale events is to point several telescopes at each patch of sky and require coincidence of detections. One can also observe in several wave-bands simultaneously, and in this way one would obtain colors for brief transients.

F Image Accumulation

F.1 Introduction

An essential task of the POI pipeline is i) to generate an accumulated image of the static sky and ii) to subtract this from each newly acquired image in order to detect transient and/or moving objects. While this appears to be simply a matter of averaging and subtraction, the problem is complicated by the following considerations

1. cosmic ray hits
2. under-sampling of the PSF
3. field distortion and misalignment of chips within the mosaic cameras
4. variations of the PSF in time and with position on the image
5. variation in the sky background
6. chip-to-chip variations in QE(λ) curves

These problems also arise, to a lesser or greater degree, in reduction of all mosaic CCD camera data, and there is a wide range of accumulated experience in tackling these problems. For example, supernovae searches have driven the development of accurate image subtraction procedures, with careful attention to the PSF modeling, and similar procedures have been developed for weak-lensing observations. Fischer & Kochanski (1994) have considered the problem of combining images with varying seeing and find a variety of different optimal weighting schemes for different applications. An iterative approach to combining images with different PSFs was proposed by Lucy & Hook (1992). Considerable effort has been applied to combining images from the heavily under-sampled WFPC images from HST, and again a diverse range of solutions have been proposed, including 'drizzling' (Hook & Fruchter 2000; Casertano et al. 2000) and Fourier image reconstruction Lauer 1999a, Lauer 1999b. The problem of determining the PSF for heavily under-sampled images has been considered in detail by Anderson & King (2000).

This diversity of solutions to the image summation problem is particularly disturbing in the present context, since it is probably not practical, and certainly not desirable to keep all of the image data. What we will need to do is *accumulate* the images in some way. Luckily, it turns out that there is a unique way to combine images with varying seeing which is optimal for *all* applications. The optimal accumulated image is

$$\varphi(\mathbf{r}) = \sum_p f_p g_p(\mathbf{r}_p - \mathbf{r})/\sigma_p^2, \tag{16}$$

where f_p is the pixel value, $\{\mathbf{r}_p\}$ are the locations of the pixels, $g_p(\mathbf{r})$ is the point spread function for the pth pixel and σ_p is the noise. Here the PSF $g(\mathbf{r})$ is the convolution of the atmospheric PSF, the pupil PSF and the pixel PSF. The latter is proportional to the probability that a photon falling a distance $\mathbf{r}$ from the center of some pixel generates an electron which is counted in that pixel. To a crude approximation, this is just a box function (i.e. unity if $|r_x|$ and $|r_y|$ are less then one half the pixel size and zero otherwise). More realistically, this will also incorporate the effects of charge diffusion, which allows photons landing outside (inside) the box to (fail

to) be registered in that pixel, and there may also be intra-pixel variations in sensitivity in front-side illuminated devices, and in the red for back-side illuminated devices. This is very general as it allows each pixel to have its own PSF and noise value. If all of the pixels in a given image have same PSF and noise then the optimal image is just

$$\varphi(\mathbf{r}) = \sum_i (g_i^\dagger \otimes f_i)_\mathbf{r}/\sigma_i^2. \tag{17}$$

where $\otimes$ denotes convolution, the dagger superscript denotes reflection $g^\dagger(\mathbf{r}) = g(-\mathbf{r})$, and where

$$f_i(\mathbf{r}) \equiv \sum_{p\subset i} f_p \delta(\mathbf{r} - \mathbf{r}_p). \tag{18}$$

This optimal accumulated image $\varphi(\mathbf{r})$ is the sum of the source images, each convolved with their individual PSFs and weighted by the inverse of the noise variance. It is a continuous function of position, but can be reasonably approximated by accumulating on a grid which is say 2 or 3 times finer than the source images. One can show that the likelihood for the actual sky is just a function of $\varphi(\mathbf{r})$, so we can be confident this is the optimal average image for all applications. It is not equivalent to any of the weighting schemes of Fischer & Kochanski (1994), who did not allow the possibility of convolving the images before combination. We stress that this only dictates what is the quantity that needs to be accumulated. There are many ways to post-process this accumulated image which can, and should, be fine tuned to particular applications. We will describe how this image can be filtered, either to remove noise correlations or Wiener filtered to enhance the visual impression of low spatial frequency features. We also describe image reconstruction, which removes the effect of discrete sampling, and for which the summed image provides the required input. Somewhat puzzlingly, however, it cannot be used as the input data for the Lucy and Hook algorithm.

F.2 Statistics of the Optimal Summed Image

The optimal summed image $\varphi(\mathbf{r})$ is a smoothed version of the raw data. Since the data are a smoothed version of the sky plus an unsmoothed noise component this means that the noise component $\varphi_N(\mathbf{r})$ of the optimal summed image is correlated with autocorrelation function $\langle\varphi(\mathbf{r}')\varphi(\mathbf{r}'+\mathbf{r})\rangle \simeq \sum_i (g_i^\dagger \otimes g_i)\mathbf{r}/\sigma_i^2$.

One can show that the signal component $\varphi_S(\mathbf{r})$ is

$$\varphi_S(\mathbf{r}) = \sum_i g_i^\dagger \otimes [c_i \times (g_i \otimes f)]/\sigma_i^2, \tag{19}$$

where $c_i(\mathbf{r})$ is a set of delta functions at the locations of the pixels. The transform of $\varphi_S(\mathbf{r})$ is

$$\varphi_S(\mathbf{k}) = \sum_i \tilde{g}_i^\star \times [\tilde{c}_i \otimes (\tilde{g}_i \times \tilde{f})]/\sigma_i^2. \tag{20}$$

Now the transform $\tilde{c} = c_i(\mathbf{k})$ of the comb function $c_i(\mathbf{r})$ is also a comb function:

$$c_i(\mathbf{k}) = e^{i\mathbf{k}\cdot\Delta\mathbf{x}_i} \sum_\mathbf{n} \delta(\mathbf{k} - \Delta k\mathbf{n}) \tag{21}$$

where $\Delta k \equiv 2\pi/\Delta x$, with Δx the pitch of the comb, and where $\mathbf{n}$ is a vector with integer valued components. The transform therefore consists of a sum of replicas (or 'satellites') of the the

true smoothed image transform on a grid of spacing Δk. If the seeing disk is much larger than the pixel size then $g(\mathbf{k})$ is very compact — width $\sim 1/\mathrm{FHHM} \ll \Delta k$ — then the satellites are well separated, and we have $\varphi_S(\mathbf{k}) \simeq \tilde{g}^\star \tilde{g} \tilde{f}$, or equivalently $\varphi_S(\mathbf{r}) \simeq g^\dagger \otimes g \otimes f$. If the PSF is not well sampled, however, the $\mathbf{n} \neq 0$ terms overlap with the zeroth order image and we have aliasing.

For a single image, the aliased and true signal are roughly equal at the 'folding frequency' $k_{\mathrm{fold}} = \pi/\Delta x$. For Kolmogorov seeing, the atmospheric attenuation at this frequency is

$$10 \log_{10}(g(k_{\mathrm{fold}})) = -4.68 \left(\frac{\mathrm{FWHM}}{\Delta x}\right)^{5/3} \mathrm{dB}. \tag{22}$$

Thus, if the pixel size is half the seeing width, for example, these spatial frequencies are suppressed by about 15dB in amplitude (30dB in power). Aliasing therefore has little effect for this sampling rate. For multiple images, the effect of aliasing is still smaller by a factor $1/\sqrt{N_{\mathrm{images}}}$. This is illustrated in figure 11 which shows the effect of aliasing for pixel size half the FWHM and the sum of 16 images.

F.3 Flat Spectrum Representation

For the sampling rate anticipated for POI, the optimal summed image is effectively just a double convolution of the object scene plus noise which is singly convolved white noise. For some applications — e.g. simple photometry packages that assume the noise is uncorrelated — this is inconvenient. It is, however, straightforward to apply a filter to render the noise spectrum flat. This simply involves dividing, in Fourier space, by an effective OTF

$$g_{\mathrm{eff}}(\mathbf{k}) = \sqrt{\sum_i |g_i(\mathbf{k})|^2/\sigma_i^2} \Big/ \sqrt{\sum_i 1/\sigma_i^2} \tag{23}$$

which is a weighted root-mean-squared of the OTFs of the individual images. This operation is operationally well-defined since it effectively only involves reversing the convolution already applied.

Applying this type of post-processing is entirely reversible, so, like $\varphi(\mathbf{r})$ the flat spectrum representation also has optimal signal to noise. Another possibility, which would be useful if one were looking for extended objects, would be to apply a Wiener filter to emphasize the frequencies at which one expects the object signal to appear.

We emphasize that the spatial filtering applied in the optimal image construction is not a Wiener filter. Wiener filtering involves a, perhaps subjective, division of data into signal and noise. The optimal image is independent of the actual image signal content. Our optimal image filter specifies the weighting to be given to different source images at each given spatial frequency. It is non-reversible and has a non-trivial, and beneficial, effect on the information content of the final image. Wiener filtering, in contrast, tells us how to weight different frequencies when combining them to make a real-space image. It affects the visual appearance of the resulting image, but has no impact whatsoever on the information content.

F.4 Image Reconstruction

While the effect of under-sampling is very weak and probably insignificant for faint objects, for very bright objects, and if the seeing is exceptional, it may be desirable to recover an image

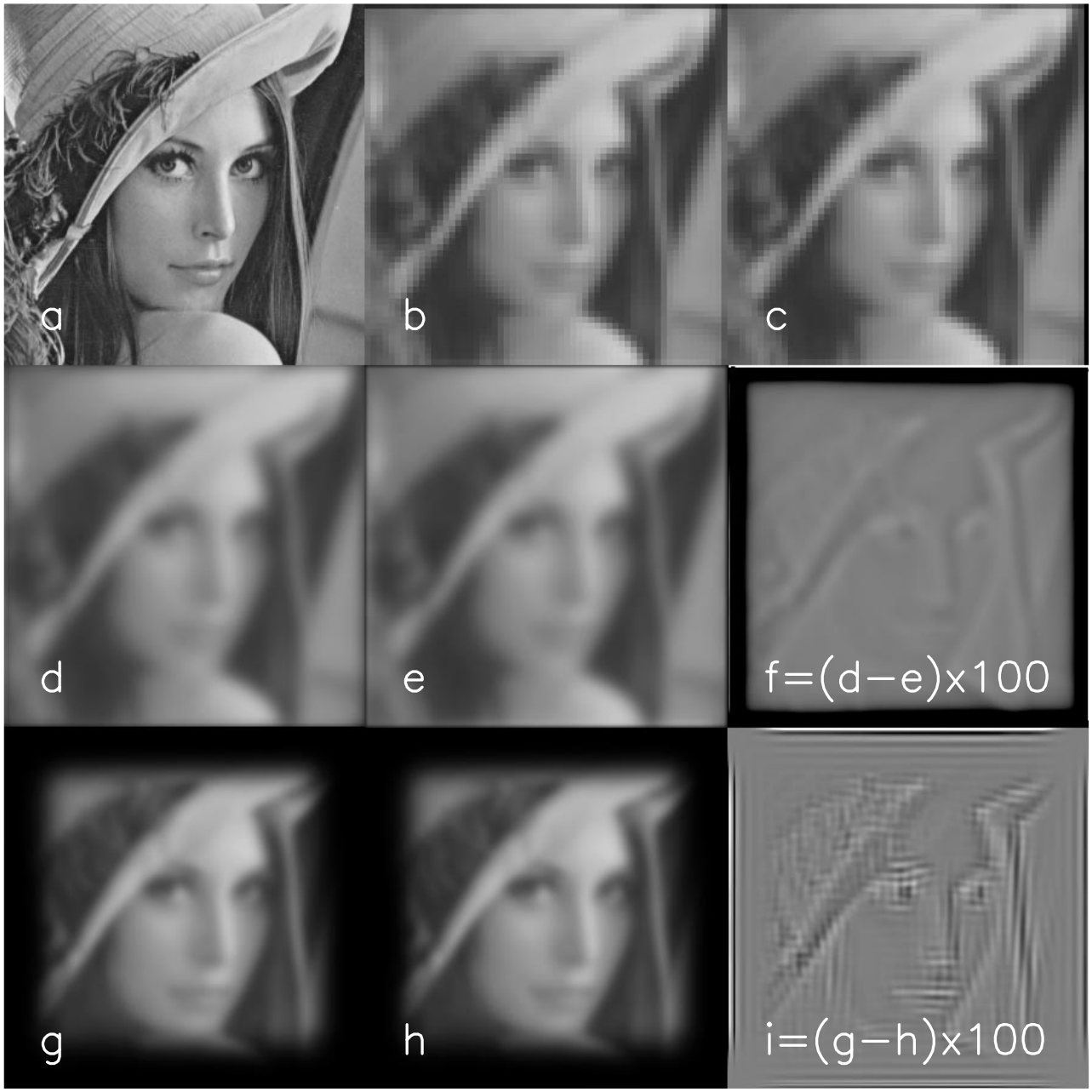

Figure 11: Aliasing in the optimal summed image for 'good seeing' conditions. Panel a shows the commonly used test image of Lena. Panels b, c show two of 16 samples of this which were made by convolving with Kolmogorov seeing; applying a random shift with interpolation; re-binning 5×5. The FWHM of the seeing was twice the final pixel size. Panel d shows the optimal sum of the 12 images, and panel e shows the original a convolved twice with the PSF (seeing and pixel response). Panel f shows the difference highly amplified. Panel g shows the result of dividing the image by $\max(|g_{\rm fs}(\mathbf{k})|, 0.01)$ in Fourier space to give a 'flat-spectrum' representation of the optimal image (though in this example the image is noise-free). Panel h shows the same filter applied to e. The low level residuals seen in panels f, i are the result of aliasing.

which is corrected for under-sampling. This can be done in a manner vary similar to that proposed by Lauer (1999a). We have generalized his approach to the case of variable PSF. The result is a set of linear equations for the transform of the reconstructed image which, in the absence of noise, exactly corrects for the discrete sampling. Interestingly, and for our purposes significantly, the data enter this formula as the transform of the optimal accumulated image (17).

F.5 Point Source Likelihood

The log-likelihood function for a point source (of flux F and position $\mathbf{r}$) is

$$\mathcal{L}(F, \mathbf{r}) = F\varphi(\mathbf{r}) - \frac{1}{2}F^2\chi(\mathbf{r}) + \text{constant} \tag{24}$$

where $\chi(\mathbf{r}) \equiv \sum_i (c_i \otimes g_i^2)_{\mathbf{r}}/\sigma_i^2$. This again depends only on the accumulated image data $\varphi(\mathbf{r})$.

Maximizing the likelihood gives the most likely flux at position $\mathbf{r}$:

$$F_{\text{ML}}(\mathbf{r}) = \varphi(\mathbf{r})/\chi(\mathbf{r}), \tag{25}$$

and substituting this back in (24) shows that the ML positions are peaks of the 'significance function'

$$\nu(\mathbf{r}) \equiv \varphi(\mathbf{r})/\sqrt{\chi(\mathbf{r})}. \tag{26}$$

In the vicinity of a peak the likelihood is a Gaussian ellipsoid (in flux-position space):

$$P(\mathbf{X})d^3X \propto \exp\left(-\frac{1}{2}\Delta X_l\left(-\mathcal{L}_{lm}\right)\Delta X_m\right)d^3X \tag{27}$$

with

$$-\frac{\partial^2\mathcal{L}}{\partial X_l \partial X_m} = \begin{bmatrix} \chi & \vdots & \varphi_i \\ \cdots & & \cdots \\ \varphi_i & \vdots & -\frac{\varphi\varphi_{ij}}{\chi} + \frac{1}{2}\frac{\varphi^2\chi_{ij}}{\chi^2} \end{bmatrix}. \tag{28}$$

This provides the full covariance matrix for errors in the flux and position in terms of the accumulated image.

For the pixel size and expected seeing for the POI, the function $\chi(\mathbf{r})$ is nearly constant (fluctuations around $1-2\%$), in which case the covariance matrix becomes diagonal, and the term involving χ_{ij}, the second derivative of χ can also be dropped.

For reasonably strong peaks (significance $\nu \geq$ a few) one can express the variance in position and flux in terms of moments of the optical transfer function:

$$\frac{\langle \Delta F^2 \rangle}{F^2} = \frac{1}{F^2\chi} = \frac{1}{\nu^2} = \frac{\Delta x^2}{F^2 \sum\limits_i \int \frac{d^2k}{(2\pi)^2} g_i^2(\mathbf{k})/\sigma_i^2}. \tag{29}$$

and

$$\langle |\Delta\mathbf{r}|^2 \rangle = \frac{\Delta x^2}{F^2 \sum\limits_i \int \frac{d^2k}{(2\pi)^2} k^2 g_i^2(\mathbf{k})/\sigma_i^2}. \tag{30}$$

These expressions (29) and (30) are quite useful for estimating sensitivity and comparing the efficiency of different instruments for the tasks of point source detection and location. Since the noise variance σ^2 scales inversely with the integration time, it follows that the figures of merit for detection and location are simply the zeroth and second moments of the OTF.

F.6 Cosmic Ray Rejection

What we are proposing here is that the accumulated image is made simply by averaging the convolved images. This is not usually done, since this averaging is not robust against cosmic rays, which can be give very high counts. More commonly, some kind of median averaging or 'avsigclip' is performed. However, for POI, we will have very good rejection of bright cosmic rays as we plan to take images simultaneously with four telescopes. Also, once we have a reasonably well determined cumulative image we will in fact be able to perform avsigclip filtering; this will be necessary to remove e.g. low-altitude satellite trails which will not get removed by the primary CR filter.

F.7 PSF Modeling

The PSFs in real telescopes vary with position on the focal plane. This is easy to cope with provided that the variation is smooth on scales at least as large as the mean separation between moderately bright stars. In CFHT12K data we typically have 50-100 samples of the PSF over each $7' \times 14'$ chip, and we find that a simple linear polynomial (for each pixel of the PSF model image) is adequate.

F.8 Anisotropy Nulling

One can rotate the PSF by 90° before convolving. This will null out quadrupole anisotropy in the PSF introduced by e.g. telescope oscillations. This does not work for all anisotropies — coma aberration, for instance, leaves a residual — but it is still a major advantage for weak lensing observations.

F.9 Choice of Dithering

The foregoing considerations impact on the choice of dithering pattern. For some applications it is advantageous to do fairly large dithers — on the order of the individual device size — in order to give a contiguously sampled image, and this certainly produces the prettiest pictures. However, if there is wide variation in the seeing, then the gaps between the chips result in discontinuities in the averaged point spread function in the accumulated images. This is bad for lensing and may also impact the static image subtraction. Another disadvantage of large dithers is that the field distortion will limit the size of sub-images over which the Fourier image reconstruction technique can be applied. If the dithers are very small compared to the individual device size then the accumulated PSF will behave smoothly, but there will be appreciable gaps in the image coverage (of tens of pixels or so). A compromise solution may be to construct a pair of summed images, each of which has small offsets so the PSF modeling and image subtraction is very precise, but with the two images shifted by 1/2 a device size so that a near continuously sampled images can be derived from the pair.

F.10 Pipeline Simulation

To test the likely performance of this optimal image combination and subtraction scheme we have implemented a pipeline, or rather a pair of pipelines, to generate test data with realistic pixel size and noise levels etc and to perform the basic pipeline reduction tasks.

We took as our model for the intrinsic sky one of the HDF images. We convolved these with Kolmogorov seeing with a realistic log-normal distribution of seeing widths. We then mapped this onto the 'focal plane' with random shifts and small rotations (to recognize the fact that we cannot point telescopes precisely). We added fake cosmic rays of random amplitudes (typically close to noise level as these are the most difficult to treat). We then sampled these with $0''.32$ pixel size and added Gaussian random noise to simulate the sky noise level expected for 60s integrations in the R-band. In the real images, we will have a large number of stars for registration and PSF measurement. Here we only simulate about 1 square arc-minute of data, so we added a grid of artificial point sources before applying seeing, with magnitudes in the range $m_R = 20 - 21$. The source image and an example simulated data image are shown in the upper panels of figure 12.

These images were generated in sets of four with identical seeing, but with different shifts, rotations, noise and cosmic rays to simulate the POI's simultaneous imaging. These were processed as follows; stars were detected with 'findpeaks' and used to determine the mapping from focal plane to sky coordinates. These stars were also used to determine the PSF. The images were re-convolved and then mapped back to sky coordinates, and a median of each set of four taken to remove cosmic rays. The resulting stream of images were then averaged. The maximum signal to noise image is shown in the lower left corner of figure 12, along with a 'flat-noise spectrum' version which has had high frequencies boosted to render the sky noise uncorrelated. Figure 13 shows the high quality of image subtraction that is possible with matched filtering.

The results of these simulations are similar to the quality of image warping and PSF modeling that we have been able to achieve routinely in reducing e.g. CFH12K data. The main difference here is that we are simulating short exposures with relatively small telescopes, so there is more noise in the star positions and shapes. This does not seem to be have impaired the results. The image subtraction for very bright saturated objects in the real images is, not surprisingly, rather poor, but such objects are not used either for registration or PSF modeling.

F.11 Summary

We have shown that there is a clearly defined optimal way to combine images of differing seeing and noise level (17). This is the quantity that the pipeline must accumulate (the software for doing all of this is already in place as this is precisely the processing we use for weak lensing analysis). This single accumulated image is in effect an exactly lossless compression of the stream of input images; along with the information regarding the locations of the pixels on the sky and their noise, PSFs etc, this image contains all of the useful information contained in the full stream of data.

We stress that this only dictates what is the quantity that needs to be accumulated. There are many ways to post-process this accumulated image which can, and should, be fine tuned to particular applications. These include Fourier filtering, either to boost high frequencies to render the noise spectrum flat, or to suppress them still further with a Wiener filter say. Another interesting type of post-processing is Fourier image reconstruction to undo the effect of discrete sampling of the images, though this is only practically useful for very bright objects. Finally, the accumulated image(s) provide one instantly with the ML locations and fluxes for point sources, and they also conveniently provide the full covariance matrix for the errors therein.

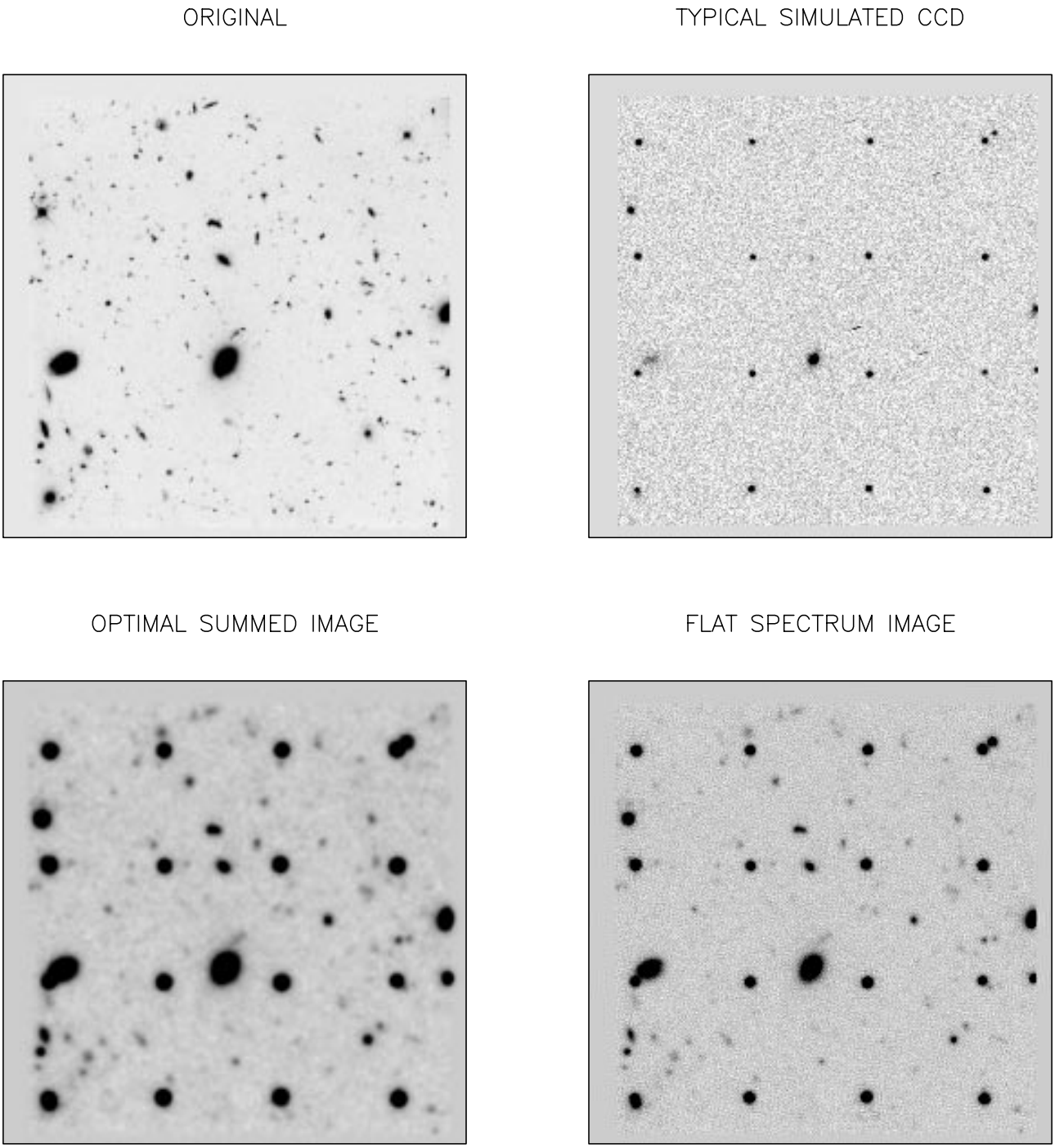

Figure 12: Upper left panel shows one WFPC2 image from the HDF. Upper right shows a simulated CCD image generated as described in the text. A few faint cosmic rays are visible as elongated streaks. The lower-left panel shows the optimally weighted combination of about 100 such exposures, and the bottom right panel shows the same image filtered to give a flat noise spectrum — this is useful for e.g. simple photometry packages that assume the sky noise is uncorrelated.

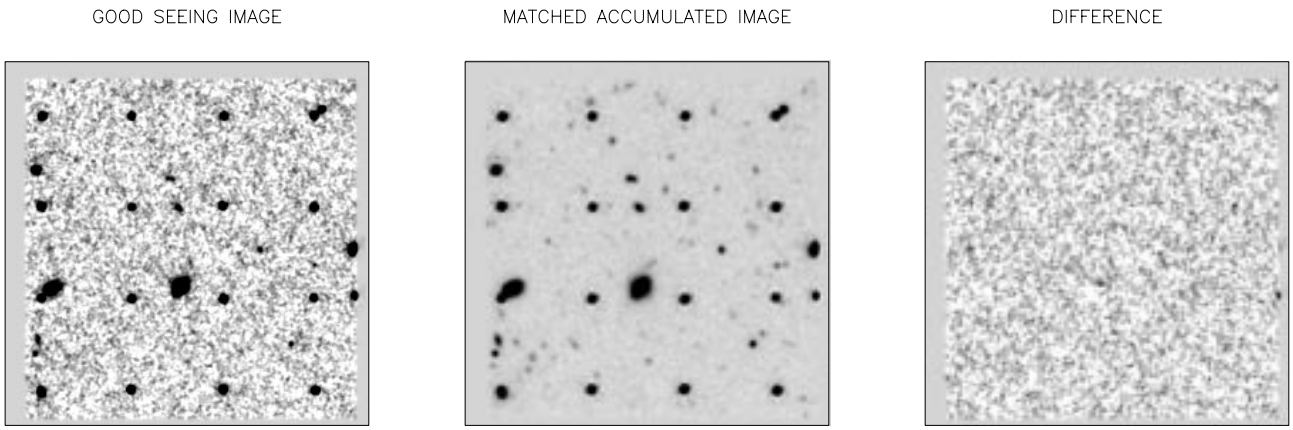

Figure 13: Illustration of subtraction of a PSF-matched image. The left panel shows one of the fake exposures from the simulation. The image has been convolved with its PSF (as this is the optimal image for detecting point sources). We chose one of the very best seeing images as these are the hardest to match. The center panel shows an image generated from the accumulated image which has been filtered in Fourier space to match the PSF. The right hand panel shows the subtraction, which is extremely good.

G Replicated or Floppy Mirrors?

Thus far we have considered exclusively conventional telescope designs. Here we briefly consider possibilities to further improve cost effectiveness with advanced technology optical elements.

Several companies are now making carbon fiber/resin composite mirrors (e.g. CMA webpage[14]). These have excellent surface quality, and are very light, which may allow a significant decrease in the cost of small telescopes.

An attractive feature of replicated composite mirrors for arrays of telescopes is that there is little penalty for generating complicated aspherical surfaces, since one only needs one mandrel.

There is some question about low-order figure errors. These may be corrected with active optics; occasionally one could take a series of out of focus images and use curvature sensing algorithms to correct for static mirror aberrations using standard curvature sensing algorithms. The alignment of the system is measured from the shift of the edges of the out of focus images.

The latter considerations apply to very thin glass mirrors, which provide a possible alternative way to decrease weight.

Active control of small telescope primaries also offers the exciting possibility of essentially complete removal of low level turbulence (this is not possible for large telescopes) so one would be limited only by the free atmosphere seeing.

Cost effectiveness of these approaches needs more consideration, but are almost certainly not viable for the pilot project.

[14] `http://home.earthlink.net/ bromeo/`

H Optical Designs

As discussed in the main text, there are many options for small, wide-field telescopes. These include the Willstrop 3-mirror designs, and also simple designs such as Couder, Schmidt and even fully refractive designs. With seed funding, all of these will be explored in detail.

H.1 Modified Bowen-Vaughan Design

We have explored some optical designs for a Ritchey-Chretien with corrector plate. One is a modification of the Bowen & Vaughan (1973) design for the 40″ at Las Campanas, with $f/5.4$ rather than $f/7$, and has two aspheric mirrors and a Gascoigne corrector plate mounted in front of the detector (which is flat). It is also very similar to the DFM design for the USNO 1.3m. The design has a compact profile.

We have also explored a 'Sloan-clone' which is similar but has a second refractive corrector mounted directly in front of the focal plane (the CCDs could be glued to the flat rear surface). The image quality for this design was not quite as good.

The physical layout for the modified Bowen-Vaughan design is shown in figure 14. Polychromatic spot diagrams are shown in figure 15 which compare favorably with those in the DMT manifesto[15]. No serious attempt at computing tolerances has been made, but we note that e.g. focus tolerance is less critical for this design than for the DMT.

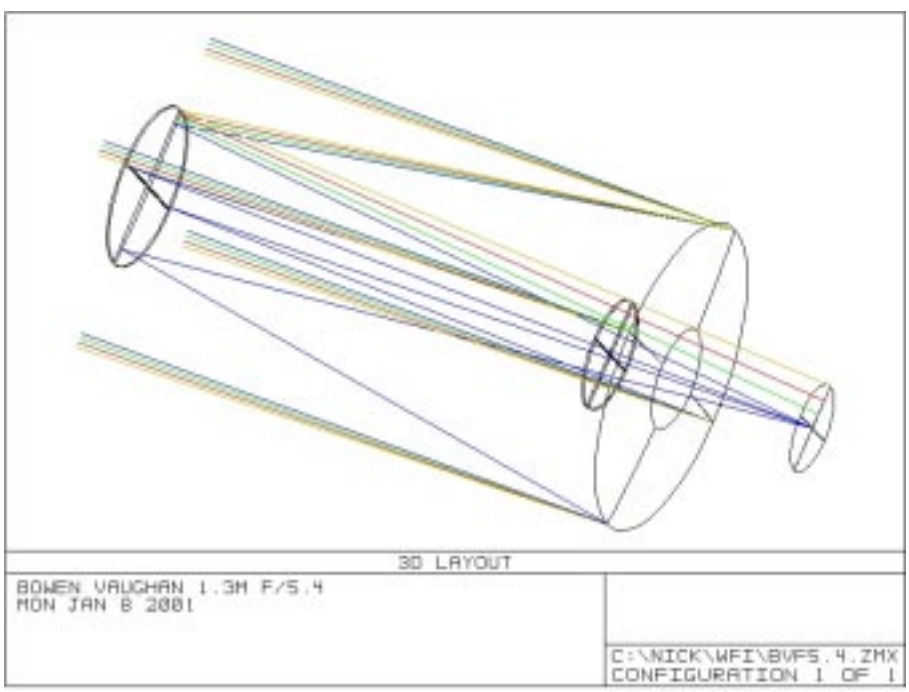

Figure 14: Physical layout of 1.3m $f/5.4$ telescope design. The optimization placed the corrector plate between the mirrors, but there is little penalty to move it back behind the primary.

[15] http://www.dmtelescope.org

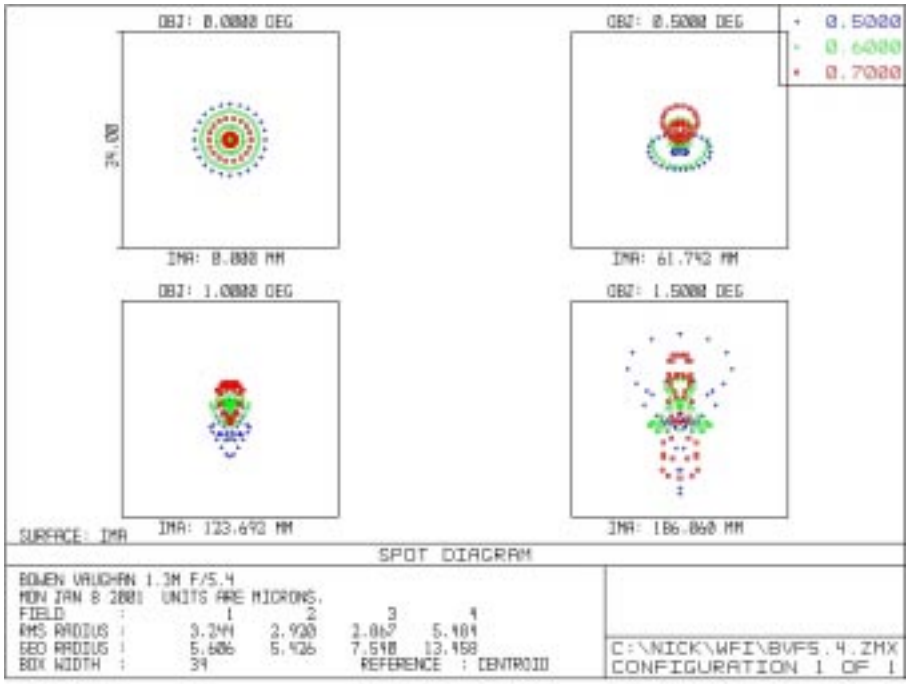

Figure 15: Spot diagrams for 1.3m $f/5.4$ telescope design. Box is $1''.0$ on a side.

H.2 Other Designs

There are various other designs — notably three-mirror designs — that need to be more carefully evaluated. Off-axis designs offer improved PSF quality. This is useful for detecting objects close to brighter neighbours and also improves the performance of fast-guiding.

I Comparison with SNAP-SAT

SNAP-SAT is a proposed wide-field imaging space telescope. Its prime science driver is to detect supernovae, but its images can also be used for weak lensing. SNAP-SAT is relevant to the POI for two reasons: First, the detector requirements for the two projects are similar. Second, it is of interest to compare the efficieny for the two approaches to wide-field imaging.

I.1 Detector Requirements

The nominal design for SNAP-SAT is a $f/10$ with a 2m diameter primary, so the plate scale is 100μm/arcsec. The nominal angular pixel scale is 0".1, so the physical pixel size is $\simeq 10\mu$m. The field of view is 1deg^2 and is required to have good sensitivity for $300 \lesssim \lambda \lesssim 1000\mu$m. To get good QE at the long-wavelength end requires thick chips, and the proposal calls for 300μ thick LBL devices.

However, this thickness of CCD severely impairs the performance of the system. Figure 16 shows the point source detection efficiency as a function of pixel size and charge diffusion scale σ. For 300μm thick devices operating at 40V the diffusion scale length is $\simeq 9.6\mu$ (measurments at Lick reported by Steve Holland), and the efficiency is only $\simeq 8\%$. This says that the effect of finite detector resolution is to increase the integration time by a factor ~ 12. The charge diffusion width is inversely proportional to the voltage V, so for 100V $\sigma \simeq 6\mu$m and the efficiency is than $\simeq 15\%$, which is better, but still punishing. This is the efficiency for $\lambda \lesssim 0.8\mu$m where the absorption length is less than the silicon thickness. At the longest wavelengths the charge carriers are created nearer to the gates and the diffusion width is slightly smaller and the efficiency is correspondingly a little higher.

It is clear from figure 16 that SNAP really needs much better detector resolution. It may be that this can be achieved by increasing the operating voltage still further (but this may cause other problems), or by going the thinner devices, even at the cost of some decrease in QE at the very red end. Smaller pixel scales would help, but the main limiting factor is charge diffusion. In this regard the requirments of SNAP and the POI are very similar. Thus, if SNAP-SAT is funded it is guaranteed that fully depleted devices with the resolution required for the POI will become available.

I.2 Performance Comparison

We now compare the relative efficiency of POI and SNAP-SAT (or other space-based wide-field imaging systems) specifically for point-source detection. To estimate the relative power of these systems one must take account of the following factors:

1. **collecting area:** Assuming SNAP-SAT primary diameter of 2.0m and similar obscuration factors, the POI collecting area exceeds that of SNAP-SAT by a factor $4\times1.3^2/2.0^2 \simeq 1.69$.

2. **solid angle:** The POI's solid angle exceeds that of SNAP-SAT (1deg^2) by a factor 7.1.

3. **duty cycle:** SNAP-SAT can observe 24 hours a day as compared to ~ 10 hours for the POI, giving SNAP-SAT an advantage of a factor ~ 2.4.

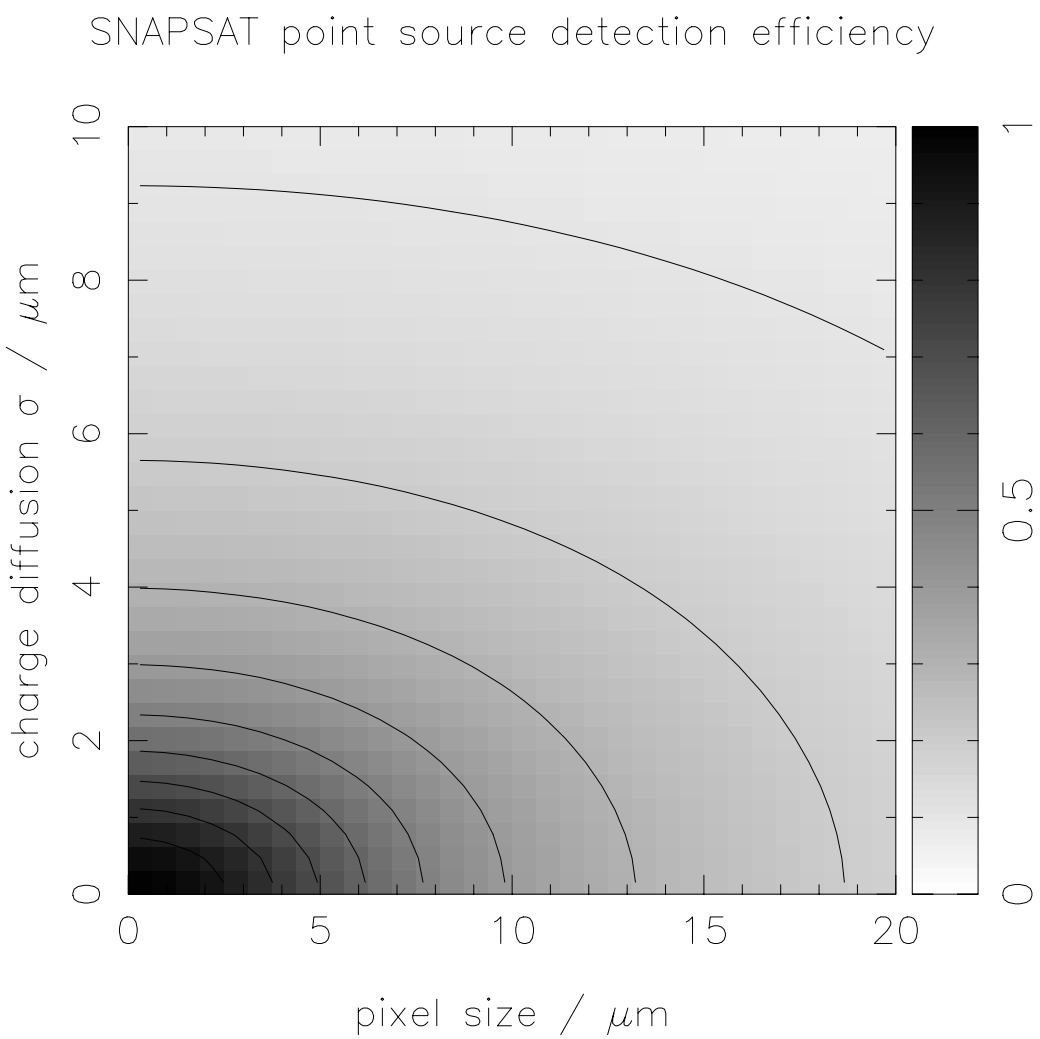

Figure 16: Efficiency of SNAP for point-source detection as a function of the pixel size and charge diffusion gaussian scale length σ. An aperture of 2m diameter with a central obscuration of 0.6m diameter was assumed. Also assumed were a focal length of 20m and observing wavelength $\lambda = 0.6\mu$m. The efficiency defined here as the inverse of the integration time required to reach a certain magnitude limit, assuming that the observations are sky noise dominated. The integration time in turn is inversely proportional to $\int d^2x\ g^2(x)$ where $g(x)$ is the PSF. Equivalently $1/t_{\rm int} \propto \int d^2k\ {\rm OTF}^2(k)$, with the total system OTF being the product of the OTFs for the pupil, pixel and charge diffusion.

4. **sky brightness:** The efficiency (science per unit time) is inversely proportional to the sky background. This is highly wavelength dependent. In the V-band, the atmospheric background is smaller than the zodiacal background which is common to both systems. However, night sky line emission becomes dominant in the near IR.

5. **atmospheric absorption:** Atmospheric extintion renders the POI inefficient in the UV.

6. **point spread function:** The efficiency is proportional to $\int d^2x\ g^2(x)$, which is a measure of the inverse area of the PSF. The SNAP-SAT proposal calls for 300μm thick devices. Operating at 100V these give a gain in efficiency, as compared to Kolmogorov seeing with FWHM = 0".6 of about a factor 6. As discussed above, the efficiency in the optical bands could be improved significantly by using thinner devices, but this would incur a loss of QE in the red.

Combining these factor gives SNAP-SAT a modest advantage of a factor ~ 3 in the visible bands; i.e. SNAP-SAT integration times are a few times smaller than needed by the POI, so SNAP-SAT can generate science a few times faster than the POI. Note, however, that the SNAP-SAT mission lifetime is much less than for POI. The real advantage of SNAP-SAT over POI is therefore in the IR and UV where the efficiency from the ground is very poor.

J Weak Lensing Efficiency

Weak-lensing (WL) is an important goal for wide-field imaging surveys. WL involves measuring the shapes of faint background galaxies. These galaxies are small and not particularly well resolved from the ground even in very good observing conditions. Here we try to quantify the gain in efficiency that can be expected from space missions such as SNAP-SAT and GEST as compared to a ground-based imager such as POI.

To do this, we take the HDF images, degrade them to mimic the effect of the smaller aperture, finite pixel size and charge-diffusion. For the POI we also allow for the effect of the atmosphere. We then add noise to simulate observations of various integration times, apply an object finder (hfindpeaks) and perform weak lensign analysis.

While the HDF images are too small to yield very useful estimates of large-scale shear, they are sufficient to give a reasonable estimate of the *uncertainty* in the shear to be expected.

J.1 Simulations

To make the simulations the HDF version 2 images were first trimmed to remove regions with excess noise close to the edges of the fields. Since there are few bright stars in the HDF, a 4×4 grid of artificial point sources with magnitudes in the range $20 < m < 21$ were introduced, to serve as a convenient reference. A PSF was constructed for each filter central wavelength by transforming the ratio of the instrument OTF to the HST OTF. For simplicity, a filled aperture pupil was assumed. The assumed diameters are given in table J.1. The images were then convolved with these PSFs to simulate the effect of the aperture diffraction.

The next step is to allow for the finite pixel size and blurring from charge diffusion. It is assumed that the deep images used for lensing will be constructed by interleaving a large number of shorter images taken on a grid of sub-pixel shifts. This gives an effectively continuously sampled image, but where the OTF contains, as a factor, the OTF of the box-like pixel function. The images were therefore convolved with the pixel box and then with a Gaussian to represent the effect of charge diffusion. Lastly, for POI, the images were convolved with an atmospheric seeing disk. This was computed assuming Kolmogorov turbulence with power chosen to give PSF with FWHM = 0".75. The parameters chosen for the various systems are given in the table.

Having made these degraded-resolution images, photon counting noise (modelled as incoherent Gaussian random noise) was added. Two values were used, to mimic the noise level for images with integration times 1/3 and 1/10 of the HDF $\sim$ 30hr integrations respectively. For the former, and in the R-band for example, this gives a 1-sigma sky fluctuation in a 1 arcsecond box corresponding to a magnitude $R = 29.1$. For comparison, this is the fluctuation level obtained in a $\simeq$ 6hr integration on the 3.6m CFHT with the CFH12K. For POI (four 1.3m telescopes) it would take $\simeq$ 11hrs to reach this sensitivity ($\simeq$ 4hrs for the shallower integrations). Integration times for GEST (one 1.3m telescope) would be about twice as long as for POI (the sky is about twice as bright from the ground) and similar for SNAP (one 2m telescope).

J.2 Shear Analysis

The degraded images were then subjected to the KSB shear analysis. This is not quite the state of the art (it does not perform an optimal weight on ellipticity) but gives very similar

results to the more sophisticated technique.

In outline, objects were detected using a variable-radius matched filter algorithm (hfindpeaks) and aperture photometry and shapes analysis was performed with apertures and kernel scale matched to the size of the objects. Objects detected at greater than 6-sigma significance were retained. Several stars (easily identifable as objects just a little larger than the grid of fake stars) were extracted and a shear polarizabilities $P = P_{\rm sh} - (P_{\rm sh}(\star)/P_{\rm sm}(\star))P_{\rm sm}$ were computed. The expectation value for the ellipticity vector is $e = P\gamma$, and near-optimal estimates of the shear are given by dividing the ellipticity e by $\overline{P}$, the average value of P for objects of similar size and magnitude. It then follws that the inverse variance in the average shear is $\langle\delta\sigma^2\rangle^{-1} = \sum \overline{P}^2/\overline{e^2}$, which is extensive in the solid angle. Dividing this by the solid angle of the HDF (approximately 3×1.55 square arcmin) gives the inverse shear variance per solid angle. Taing the inverse of the square root of this number gives the uncertainty in the mean shear estimated from unit solid angle (one square degree here).

The results of the simulations are shown in figure 17. The panels on the left/right show the results for the shallow/deep simulations respectively. The symbols indicate the system (P=POI, G=GEST, S=SNAP) and the colors indicate the filter (F450W=blue, F606W=green, F814W=red). From the top, the panels show i) the number of galaxies detected at $>$ 6-sigma ii) the inverse shear variance iii) the median redshift and iv) the mean redshift. The redshift statistics were calculated using Sawicki's photometric redshift estimates.

These results show that, as expected, the sharper PSF for the space observatories allows one to detect more objects, and this gives an increase in the precision. However, there is little change in the typical redshift of the galaxies — apparently the extra objects are found by probing fainter into the luminosity function rather than probing greater depth. The results show that for the ground based observations the shear precision is fairly insensitive to the integration time once one reaches this depth (point source detection limit $\sim R = 26$).

If the goal is to determine the cosmic shear variance, or equivalently the mass power spectrum, the figure of merit is proportional to the square of the inverse shear variance times the number of fields measured. Put another way, the final precision in the cosmic shear variance for cells of some scale is the shear variance for one cell divided by square root of the number of cells. Thus, if the inverse shear variance increases less rapidly than the square root of the integration time (as seems to be the case for all these systems at these rather faint magnitudes) then it is more profitable to measure more fields with poorer precision.

If we restrict attention to the shallower simulations, we find that the PSF improvement confers an advantage (over ground based observing) of about a factor 2 for GEST and 4 for SNAP. To obtain the total system efficiency one needs to factor in the collecting area; the field of view and the duty cycle (the fraction of time the system is taking useful data for lensing). For ground based surveys one should divide by the increased sky brightness from air-glow; roughly a factor 2 in the R band, but rising to ~ 5 in the I.

These numbers are for power spectrum — or more genererally second order statistic — measurement only. For higher order statistics things are different. In the mildy non-linear

system	diameter	pixel size	diffusion scale
POI	1.3m	$0''.28$	$0''.14$
GEST	1.3m	$0''.20$	$0''.10$
SNAP	2.0m	$0''.12$	$0''.06$

regime, where one is trying to measure relatively small departures from a Gaussian distribution it may be that precision is more important than area. Probing strong non-linearity (i.e. cluster searches) may be different again.

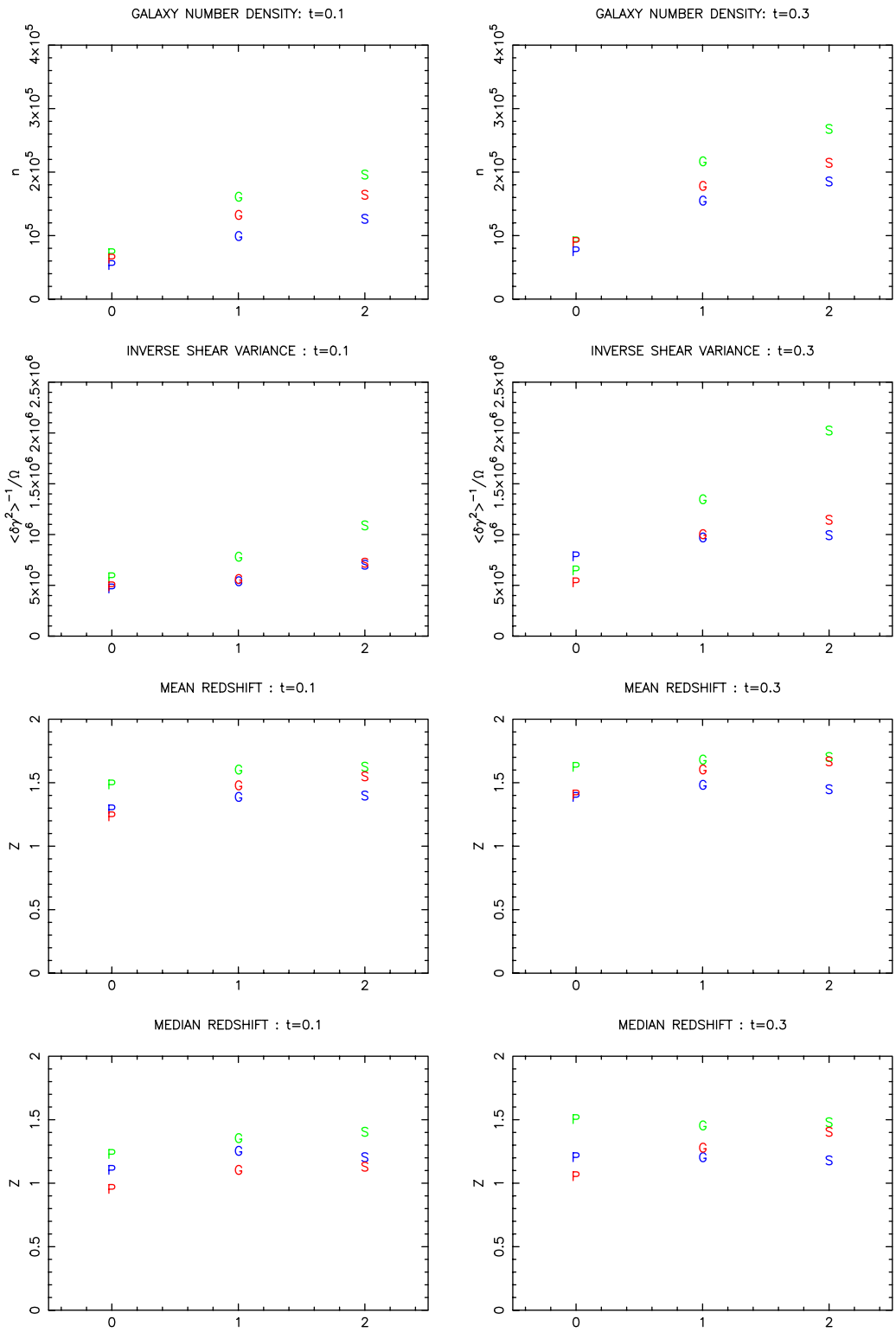

Figure 17: Efficiency for WL observations from simulations using degraded versions of the HDF.

K Terrestrial Satellites and Space-Junk

The POI can be used to detect and monitor satellites and/or space-junk in orbit about the Earth. Here we estimate the sensitivity for this task.

K.1 Bright Satellites

Modeling a satellite as a reflecting sphere of radius r, and assuming it lies outside of the earths shadow, the absolute magnitude is $M \simeq M_\odot - 5\log_{10}(r/2\mathrm{AU})$. Since $M_\odot \simeq 5$ the apparent magnitude at distance D is

$$m(D,r) \simeq 19.0 - 5\log_{10}(r/\mathrm{cm}) + 5\log_{10}(D/R_\oplus) \tag{31}$$

where $R_\oplus \simeq 6,380\mathrm{km}$ is the radius of the earth.

The angular velocity of a satellite in circular orbit passing overhead at altitude D is

$$\dot{\theta} = \frac{v}{D} = \frac{1}{D}\sqrt{\frac{GM_\oplus}{R_\oplus + D}} \simeq \frac{4^\circ.25}{\mathrm{min}} \times \begin{cases} \frac{R_\oplus}{D} & D \ll R_\oplus \\ \left(\frac{R_\oplus}{D}\right)^{3/2} & D \gg R_\oplus \end{cases} . \tag{32}$$

Assuming seeing with FWHM $\simeq 0''.6$, and integration time of 1min, the limiting magnitude for 5-sigma detection of a static point source is $m_V \simeq 24.0$. More generally, the limiting v-magnitude is $m_{\mathrm{lim}} = 24.0 - 2.5\log(\mathrm{FWHM}/0''.6) + 1.25\log(t_{\mathrm{exp}}/1\mathrm{min})$. Now a satellite moves one resolution element (or 'resel') in a time

$$t_1 = \frac{\mathrm{FWHM}}{\dot{\theta}} \simeq 3.9\times 10^{-5}\mathrm{min}\left(\frac{\mathrm{FWHM}}{0''.6}\right) \times \begin{cases} \frac{D}{R_\oplus} & D \ll R_\oplus \\ \left(\frac{D}{R_\oplus}\right)^{3/2} & D \gg R_\oplus \end{cases} . \tag{33}$$

The measured magnitude of a single resel of the trail is $m_1 = m(D,r) - 2.5\log(t_1/t_{\mathrm{exp}})$ and equating this to the limiting magnitude yields a limiting size

$$r_1 \simeq 16\mathrm{cm}\left(\frac{t_{\mathrm{exp}}}{1\mathrm{min}}\right)^{1/4} \times \begin{cases} \left(\frac{D}{R_\oplus}\right)^{1/2} & D \ll R_\oplus \\ \left(\frac{D}{R_\oplus}\right)^{1/4} & D \gg R_\oplus \end{cases} . \tag{34}$$

This is the size of satellite for which a single resel sized segment of the trail can be detected at the 5-sigma level. This formula tells us that the POI can detect satellites of size $\gtrsim 20$cm out to geosynchronous orbit at a fairly high degree of significance. Note that the limiting size is a very weak function of distance. It is also interesting to note that the limiting size is independent of the seeing, and *increases* with increasing integration time.

K.2 Faint Satellites

Objects of size considerably smaller than r_1 given by (34) can also be detected by the POI by more sophisticated object detection analysis. Since the satellites leave a long trail, by convolving the images with a series of template trails (of various lengths and orientations) one can detect trails for which the individual resels are too faint to be detected. If we can find a template that matches a trail of length N resels then the limiting flux is reduced by a factor $\sqrt{N}$ and

the limiting size is reduced, relative to (34), by a factor $N^{1/4}$. Note that satellites are often spin-stabilized, or may be tumbling, so the trails will, in general, pulsate.

More specifically, in the POI pipeline, the cumulative image of the static sky is subtracted from each image, and we will assume that streaks are detected from these images which should be blank aside from transient or other moving objects (and possibly cosmic rays, see below). We will assume that streaks are detected by convolving the images with set of straight-line template streaks and locating peaks. We do not need to sample all possible streak lengths; it suffices to sample a logarithmically spaced set of lengths. However, for streaks of length N resels there are $\sim N$ distinguishable angles we need to try, so for very long streaks the task becomes computationally very demanding. Even using the FFT to perform convolutions, the number of operations required to search for trails of length N in an image of size M is on the order of NM^2 (times logarithmic factors which we will ignore). Equivalently, we need to perform $\sim N$ operations per pixel of data. We do not need to perform the convolutions on the complete image — this can be broken up into chunks of size $\sim N$ for convenience.

Even with infinite computing resources, there is a limit to how long a streak can be searched for. We have seen that for objects at distance $D \simeq R_\oplus$, the trail length is roughly equal to the POI FOV of 3°, or about $18,000$ resels long. However, for such orbits the *curvature* of the trails is typically quite important (see §K.7 below). The worst case is for an object transiting with distance $D = R_\oplus$ at zenith distance $z = 60^\circ$, for which the deviation from a tangent great circle at the field center amounts to about $20''$. For such objects the truly optimal search algorithm would involve searching for a huge number of possible *arcs*. However, even for these maximally curved trails, the trails can be considered to be straight over lengths of the order of $\sim 1000 - 2000$ resels, so a search for trail segments of this size would still yield a substantial decrease in limiting object size.

Our images contain $\sim 10^{8-9}$ resels, so to search for streaks up to say 1000 resels long requires $\sim 10^{5-6}$ two-dimensional 1K $\times$ 1K FFTs. Off-the shelf DSP boards can perform one such FFT in ~ 0.1s, or about 1000 FFTs per exposure + readout time, so about 100-1000 boards would be required to keep up with the data flow in real time. This is a very rough estimate, but suggests that this is probably doable with current technology. Note that it is only for the very faintest objects at the absolute limit of detection that one needs to search for long trails. Bright objects can be detected in short trail segments, for which the computation is relatively inexpensive.

If we choose to search for trails up to length $N_{\rm max}$ there is a critical distance $D_{N_{\rm max}}$ such that $t_{\rm exp}/t_1(D_{N_{\rm max}}) = N_{\rm max}$; for more distant objects the full length of the trail is less than $N_{\rm max}$ resels long. For plausible values of $N_{\rm max}$ this critical distance lies in the domain $D \gg R_\oplus$ and is given by

$$D_{N_{\rm max}} = R_\oplus \left(\frac{1}{N_{\rm max}} \frac{t_{\rm exp}}{\sqrt{GM_\oplus/R_\oplus^3}} \frac{1}{\rm FWHM} \right)^{2/3} \simeq 8.7 \left(\frac{t_{\rm exp}}{1{\rm min}} \right)^{2/3} \left(\frac{N_{\rm max}}{1000} \right)^{-2/3} \left(\frac{0''.6}{\rm FWHM} \right)^{2/3} R_\oplus. \tag{35}$$

The limiting detectable object size is given by multiplying r_1 given by (34) by $N^{-1/4}$ with $N = N_{\rm max}{\rm min}(1, (D/D_{N_{\rm max}})^{-3/2})$. This gives

$$r_{N_{\rm max}} \simeq \begin{cases} 2.84{\rm cm} \left(\frac{N_{\rm max}}{1000}\right)^{1/4} \left(\frac{t_{\rm exp}}{1{\rm min}}\right)^{1/4} \begin{cases} \left(\frac{D}{R_\oplus}\right)^{1/2} & D \ll R_\oplus \\ \left(\frac{D}{R_\oplus}\right)^{1/4} & R_\oplus \ll D \ll D_{N_{\rm max}} \end{cases} \\ 1.18{\rm cm} \left(\frac{\rm FWHM}{0''.6}\right)^{1/4} \left(\frac{D}{R_\oplus}\right)^{5/8} & D \gg D_{N_{\rm max}} \end{cases}. \tag{36}$$

The limits in these three regimes are shown graphically in figure 18. As an example, for an object at the distance of the moon ($D \simeq 60R_\oplus$), a 1-minute exposure gives a trail ~ 70 resels long, and a limiting size of $r_{\rm lim} \sim 15$cm, or about the size of a basketball.

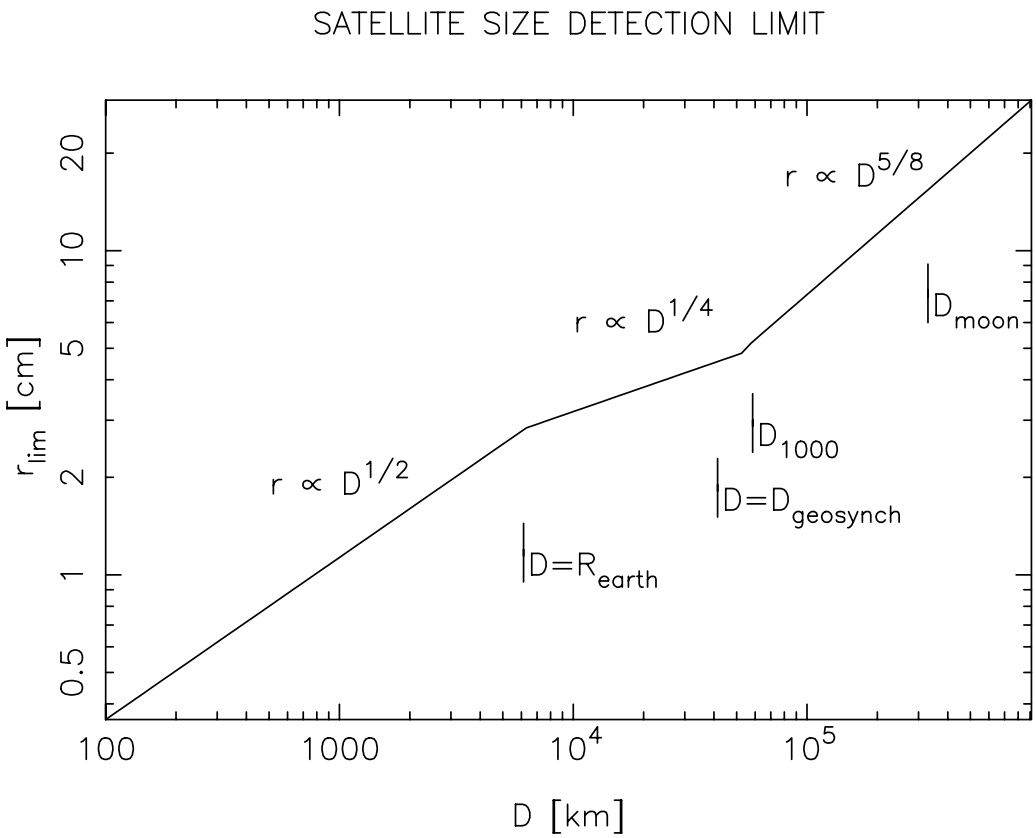

Figure 18: Limits on the detectable size of satellites with the POI as given by (36). We have assumed here FWHM $= 0''.6$, 1 minute exposure time, and a search for trails up to 1000 resolution elements long. The distance D_{1000} is the distance for which the trail is 1000 resolution elements long.

K.3 Depth of Field

The POI's small apertures give great depth of field; if we focus at infinity, then small objects remain effectively point-like down to distance $D \simeq D_{\rm primary}/{\rm FWHM} \simeq 300{\rm km}(0''.6/{\rm FWHM})$. At lower altitude the trails will become blurred. However, according to (36) this does not affect the limiting size since $r_{N_{\rm max}}$ is independent of the FWHM for $D \ll R_\oplus$. The reason for this peculiar behavior is that in this regime we are limited not by the actual data, but by our assumed limit on computational power. For poor seeing (or very low altitude satellites) one would re-bin the data to a coarser resolution and thus be able to search for longer trails. Note that for very low orbits, the curvature of the trails becomes negligible.

Another slight complication is that the trails in the images from the different telescopes will be displaced by slightly. For a baseline of 10m, for example, the shift is comparable to the seeing disk size for altitude of $\simeq 3000$km, so the shift is appreciable for lower altitude. This allows one to approximately determine the object distance by triangulation.

Bright objects at lower altitude would be flagged by the reduction pipeline as cosmic rays (CRs), and so one would want to search for these using images without CR rejection applied. The presence of CRs will introduce a noise background in the convolution results, so one would need to perform a filter to check the reality of candidate trails. This problem can be ameliorated by clipping the images, as the CRs — unlike the trails — tend to be very small but very bright. Faint low altitude objects would not trigger CR detection, so these, and high altitude objects, are best detected in images which have had CRs removed.

K.4 Orbit Determination

To determine the orbit of a satellite we need to see both ends of the trail. For 1 min exposures and 3° FOV this is only possible if $D \gtrsim R_\oplus$. In principle, lower altitude objects can be determined if one were to say periodically flick the shutter closed, as this would 'time-stamp' the trails.

K.5 Angular Resolution

The resolving power is atmosphere limited, giving a limit on resolvable size of $r \sim 2 \times 10^{-6} D$ or about 60m at geosynchronous orbit. It is possible to improve this slightly by deconvolution or 'super-resolution' techniques.

K.6 Dedicated Searches

So far, we have assumed that the search is performed serendipitously using the POI science data. In principle, one can obtain smaller object size detection limit by tracking the object and thus reducing the 'trailing loss'. However, this requires that one know the orbit of the object and would be an extremely wasteful use of a telescope with a 3° FOV. An exception is for orbits in near equatorial geosynchronous orbits, for which an an effective strategy is to hold the telescopes fixed. Background objects will be smeared out in the E-W direction, and can be removed either by standard flat-fielding techniques or, more precisely but with a little more effort, by subtracting the predicted smeared trails from the accumulated static images.

The greatest sensitivity is obtained for particles exactly in the equatorial plane as these will appear as point sources with no 'trailing loss'. The limiting magnitude for detection of a static object at the 5-sigma significance level in a 60s integration is $m_V \simeq 24$. This corresponds to objects only a few mm in radius.

Satellites at geosynchronous altitude but with orbits out of the equatorial plane will not remain fixed in such scans, but for small inclinations their motion will be smaller than for a serendipitous search program. The detectable object size however scales only as the 1/4 power of the angular speed, so the gain is marginal.

K.7 Curvature of Trails

Objects will generally appear as curved trails in long exposures. This curvature complicates the search strategy, or, if one searches only for effectively straight arc segments, this limits the length of segment one can search for. If we observe an object in a circular orbit of radius R as

it transits at zenith angle z, then the deviation from the tangent to the trail at the field center is

$$\theta_\perp = \frac{\alpha}{2}\theta^2 \tag{37}$$

where θ is the distance from the field center and the curvature parameter is

$$\alpha = \frac{R_\oplus \sin z}{R^2}\left[\sqrt{R^2 - R_\oplus^2 \sin^2 z} - R_\oplus \cos z\right]. \tag{38}$$

The curvature of course vanishes for objects which pass directly overhead ($z = 0$). The curvature also tends to zero for both very high ($R \gg R_\oplus$) and very low ($R - R_\oplus \ll R_\oplus$) orbits. The radius of the most highly curved orbits which transit at zenith angle z is found by solving $\partial\alpha/\partial R = 0$ which yields

$$R = R_\oplus\sqrt{2(1+\cos z)} \tag{39}$$

with curvature

$$\alpha_{\max}(z) = \frac{\sin z}{2(1+\cos z)}. \tag{40}$$

The absolute worst case is obtained by solving $d\alpha_{\max}/dz = 0$. The relevant root of this equation is $z = 60°$, for which the curvature is $\alpha = 1/\sqrt{12}$ and the radius is $R = \sqrt{3}R_\oplus$.

For this maximally curved trail, the deviation from a great circle is $\theta_\perp \simeq 20''(\theta/1°.5)^2$, which, at the edge of the nominal POI field of view ($\theta = 1°.5$) is much greater than the atmospheric seeing (FWHM $\sim 0''.6$). The distance to this satellite turns out to be $D = R_\oplus$ and the angular velocity is $\dot\theta \simeq 3°/\text{min}$ which means that, purely coincidentally, such a satellite moves about the POI FOV diameter in one nominal 1 minute exposure time. This means that curvature is quite significant these objects. Conversely, segments of these trails can be considered to be effectively straight lines ($\theta_\perp <$ FWHM) only for segment length $\theta = 2\sqrt{2\text{FWHM}/\alpha} \simeq 0°.5\sqrt{\text{FWHM}/0''.6}$. A segment of this length will deviate from a minimum deviation straight line fit by FWHM/2. This length is about $3,000$ resolution elements for FWHM $= 0''.6$.

There is another way that curvature can arise; since we must map the images onto some planar projection of the sky; even if the trail is a great circle on the sky, it will not appear as a straight line in the projection unless it passes through the field center. For the stereographic projection, the deviation of a the projection of a great circle from the tangent line is, for small FOV,

$$\theta_\perp = \theta(\theta')^2/4 \tag{41}$$

where θ is the perpendicular distance to the field center, θ' is the distance along the line, and angles are in radians. Taking $\theta = \theta' = 1°.5$, i.e. the maximum possible deviation for a square field of half-side $1°.5$, the deviation is $\theta_\perp \simeq 4.5 \times 10^{-6} \simeq 0''.9$. This is not entirely negligible, but is fairly small and is much less than the (maximal) deviation calculated above.

K.8 Conclusions

The limiting sizes calculated above (and summarized in figure 18) are the minimum compatible with sky noise considerations. They assume that the static sky subtraction is very good etc. and they are computed for a rather low 5-sigma detection threshold. If the real limiting magnitude were a factor 10 higher then the limiting size increased by a factor 3. Also, for low orbits, we have assumed a rather expensive computation — searching for trails up to ~ 1000 resels

long — and decreasing this by a factor 16 say would increase the size limit by perhaps another factor 2. Even with these conservative assumptions we find that any artificial satellite greater than ∼10cm in size should be quite easily detectable by the POI, and the luminosity of larger satellites can be measured to a high degree of precision.

References

Anderson, J., & King, I. R. 2000, PASP, 112, 1360

Angel, R., Lesser, M., Sarlot, R., & Dunham, E. 2000, in ASP Conf. Ser. 195: Imaging the Universe in Three Dimensions, 81

Bowen, I., & Vaughan, A. 1973, Appl. Opt., 12, 1430

Casertano, S., et al. 2000, AJ, 120, 2747

Dark Matter Telescope Web Site. 1999, `http://www.dmtelescope.org`

Fischer, P., & Kochanski, G. P. 1994, AJ, 107, 802

Gehrels, T., Matthews, M. S., & Schumann, A. M. 1994, Hazards due to comets and asteroids (Space Science Series, Tucson, AZ: University of Arizona Press, —c1994, edited by Gehrels, Tom; Matthews, M.S.; Schumann, A.M.)

Groom, D. E. 2000, Proc. SPIE, 4008, 634

Groom, D. E., Eberhard, P. H., Holland, S. E., Levi, M. E. ., Palaio, N. P., Perlmutter, S., Stover, R. J., & Wei, M. 2000, in Workshop on Optical Detectors for Astronomy, Garching, Germany, 13-16 September 1999????

Hook, R. N., & Fruchter, A. S. 2000, in Astronomical Data Analysis Software and Systems IX, ASP Conference Proceedings, Vol. 216, edited by Nadine Manset, Christian Veillet, and Dennis Crabtree. Astronomical Society of the Pacific, ISBN 1-58381-047-1, 2000, p. 521., Vol. 9, 521

Kaiser, N., Tonry, J., & Luppino, G. 2000, PASP, 112, 768

Lauer, T. R. 1999a, PASP, 111, 227

Lauer, T. R. 1999b, PASP, 111, 1434

Lucy, L. B., & Hook, R. N. 1992, in ASP Conf. Ser. 25: Astronomical Data Analysis Software and Systems I, Vol. 1, 277

Melsheimer, F. M., & MacFarlane, M. J. 2000, Proc. SPIE, 4003, 456

Racine, R. 1996, PASP, 108, 372

Subaru Suprime-Cam Web Site. 1999, `http://indus.astron.s.u-tokyo.ac.jp/works/suprime/index.h`

Tonry, J., Burke, B. E., & Schechter, P. L. 1997, PASP, 109, 1154

Tyson, A., & Angel, R. 2000, in New Era of Wide-Field Astronomy, ed. R. Clowes, A. Adamson, & G. Bromage??

Vista Web Site. 1999, `http://www-star.qmw.ac.uk/~jpe/vista`

WFHRI Web Site. 1999, `http://www.ifa.hawaii.edu/~kaiser/wfhri`

Willstrop, R. V. 1983, MNRAS, 204, 99P

Willstrop, R. V. 1984, MNRAS, 210, 597